Article

First Direct Insight into the Local Environment and Dynamics of Water Molecules in the Whewellite Mineral Phase: Mechanochemical Isotopic Enrichment and High-Resolution ^{17}O and ^{2}H NMR Analyses

Ieva Goldberga,* Nicolas Patris, Chia-Hsin Chen, Emilie Thomassot, Julien Trébosc, Ivan Hung, Zhehong Gan, Dorothée Berthomieu, Thomas-Xavier Métro, Christian Bonhomme, Christel Gervais, and Danielle Laurencin*

ACCESS | 📊 Metrics & More | 📖 Article Recommendations | 🆂🅸 Supporting Information

ABSTRACT: Calcium oxalate minerals of the general formula $CaC_2O_4 \cdot xH_2O$ are widely present in nature and usually associated with pathological calcifications, constituting up to 70−80% of the mineral component of renal calculi. The monohydrate phase ($CaC_2O_4 \cdot H_2O$, COM) is the most stable form, accounting for the majority of the hydrated calcium oxalates found. These mineral phases have been studied extensively via X-ray diffraction and IR spectroscopy and, to a lesser extent, using ^{1}H, ^{13}C, and ^{43}Ca solid-state NMR spectroscopy. However, several aspects of their structure and reactivity are still unclear, such as the evolution from low- to high-temperature COM structures (LT-COM and HT-COM, respectively) and the involvement of water molecules in this phase transition. Here, we report for the first time a ^{17}O and ^{2}H solid-state NMR investigation of the local structure and dynamics of water in the COM phase. A new procedure for the selective ^{17}O- and ^{2}H-isotopic enrichment of water molecules within the COM mineral is presented using mechanochemistry, which employs only microliter quantities of enriched water and leads to exchange yields up to ∼30%. ^{17}O NMR allows both crystallographically inequivalent water molecules in the LT-COM structure to be resolved, while ^{2}H NMR studies provide unambiguous evidence that these water molecules are undergoing different types of motions at high temperatures without exchanging with one another. Dynamics appear to be essential for water molecules in these structures, which have not been accounted for in previous structural studies on the HT-COM structure due to lack of available tools, highlighting the importance of such NMR investigations for refining the overall knowledge on biologically relevant minerals like calcium oxalates.
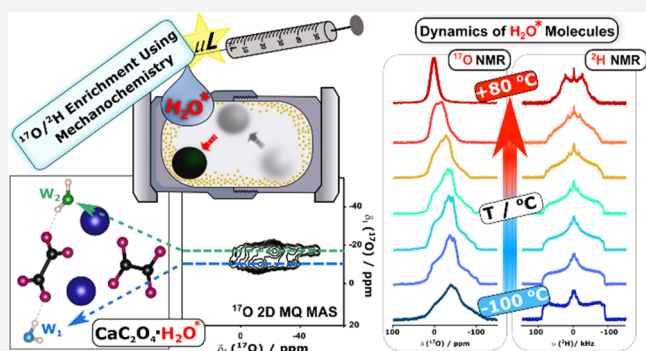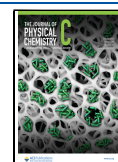
INTRODUCTION

Calcium oxalates are a common family of minerals found in natural environments, such as the soils and plants of marine and lake sediments (lignite, algae, lichens, and fungi).[1−3] They can form through biomineralization processes in living organisms and have been extensively studied within kidney stone disease.[4−6] These minerals are present in nature as three crystalline hydrated phases: whewellite ($CaC_2O_4 \cdot H_2O$, calcium oxalate monohydrate, COM),[7,8] weddellite ($CaC_2O_4 \cdot (2 + x)H_2O$, calcium oxalate dihydrate, COD),[9] and caoxite ($CaC_2O_4 \cdot 3H_2O$, calcium oxalate trihydrate, COT),[10] where the dihydrate and trihydrate phases are known to be less stable and transform to the monohydrate phase over time.[11−14] Other phases, like amorphous calcium oxalates, have also been observed in synthetic samples,[15−19] and recently, their role in kidney stones has been

investigated.[20] Moreover, synthetic anhydrous forms are known, which tend to rehydrate quickly to reform the monohydrate phase under ambient conditions.[16,21] Overall, studies on the hydration/dehydration transformations (Figure 1a) show that the monohydrate is the most stable form, explaining why it is the most prevalent component of oxalate-based kidney stones.[1,5,22−26] While the investigations on the phase transitions highlight the importance of water in the crystallization processes, its exact role in the formation and the

ACS Publications
© 2022 The Authors. Published by
American Chemical Society
12044
https://doi.org/10.1021/acs.jpcc.2c02070
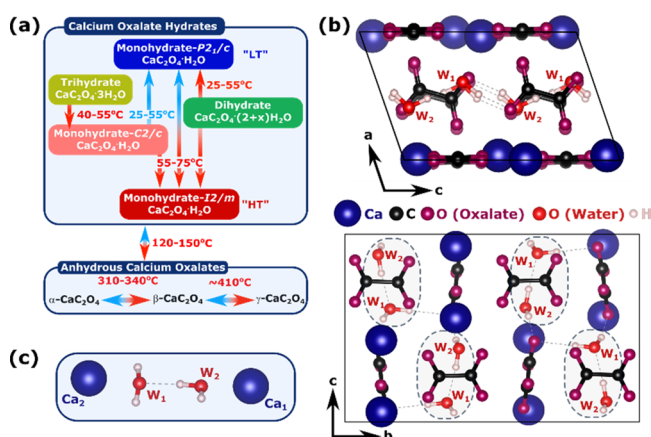J. Phys. Chem. C 2022, 126, 12044−12059

Figure 1. (a) Schematic representation of chemical and structural evolutions between calcium oxalate minerals. The red arrows indicate heating, and the blue arrows indicate cooling. The evolution shown for the oxalate minerals is based on what has been proposed by Izatulina et al.[24] Abbreviations "LT" and "HT" refer to low- and high-temperature structures. (b) Crystal structure of calcium oxalate monohydrate (COM, $CaC_2O_4 \cdot H_2O$), with two different water environments highlighted in the structure as W_1 and W_2 and shown clearly in panel c. The images of crystal structures were produced using the VESTA software[46] and the neutron diffraction crystallographic data reported by Daudon et al. (CCDC: 1428017).[31]

mechanisms of phase convergence are still unclear, meaning that further structural analysis is still needed.

The structures of calcium oxalates and even kidney stones have been studied extensively using X-ray and/or neutron diffraction,[7−11,24,27−29] scanning electron microscopy (SEM),[18,27,30,31] infrared (IR) and Raman spectroscopies,[11,12,16,32−35] and more recently solid-state NMR spectroscopy.[16,19,36−41] Moreover, computational studies have been carried out to help understand the polymorphism of anhydrous and monohydrate phases and to rationalize the shapes of the crystallites.[42−44] The X-ray diffraction (XRD) studies of COM have shown that this phase has low- and high-temperature structures, denoted as LT and HT, respectively. The most stable and known form, the LT phase, has a monoclinic $P2_1/c$ space group composed of two alternating layers: one consisting of calcium and oxalate ions and the other consisting of oxalate ions and water molecules; both layers are linked by ionic interactions and hydrogen bonds (Figure 1b). The crystal structure consists of two crystallographically nonequivalent Ca^{2+} cations, two oxalate anions, and two water molecules (denoted as W_1 and W_2). These water molecules form dimers where W_1 is hydrogen-bonded to two oxalate oxygens and W_2 is hydrogen-bonded to one oxalate oxygen and the W_1 molecule (Figure 1b,c). IR spectroscopy has further confirmed the presence of two kinds of water molecules where five well-resolved bands in the O−H stretching region (3500−3000 cm^{-1}) have been observed.[32,33,35] The HT form of whewellite is induced during a temperature increase between 55 and 75 °C, where slight atomic positional shifts are observed and the lattice type changes from primitive to I-centered.[24,45] Through computational studies, it has been proposed that HT-COM possesses a statistical $I2/m$ space group symmetry where the water molecules' positions are considered disordered and can occupy four orientations.[44] The other temperature transitions reported for calcium oxalates are shown in Figure 1a, highlighting the structural flexibility of these phases.

Since solid-state NMR can provide detailed information on the local environment of atoms, it has recently been used to look at calcium oxalate structures via ^{43}Ca, ^{1}H, and ^{13}C NMR. Calcium-43 is a particularly insensitive quadrupolar nucleus ($I = 7/2$) due to its low natural abundance (~0.14%) and low gyromagnetic ratio ($\gamma = -1.8028 \times 10^7$ rad s^{-1} T^{-1}). Therefore, (ultra-)high fields and large amounts of sample are required to study ^{43}Ca by NMR at natural abundance,[36,39] which can be an issue especially when it comes to analyzing more complex compositions of minerals of pathological relevance, like renal stones.[37,38] Nevertheless, natural abundance ^{43}Ca MAS NMR spectra have been recorded for all three crystalline hydrates, where two calcium sites have been observed for the LT-COM phase and one for the COD and COT phases, as expected from their crystal structures.[36−38] In contrast to calcium-43, ^{1}H is a highly sensitive spin-1/2 nucleus for NMR ($\gamma = 2.6752 \times 10^8$ rad s^{-1} T^{-1}), but it can suffer from a lack of resolution in the solid state, especially in cases of strong $^{1}H-^{1}H$ dipolar couplings. For COM, using a homonuclear decoupling pulse sequence (DUMBO), the ^{1}H NMR spectrum was recorded, showing only one signal centered at 5.26 ppm at room temperature, which was attributed to an averaging of the water molecules' ^{1}H resonances.[37] Upon lowering the temperature to 100 K, four proton environments could be resolved using a heteronuclear NMR experiment (FSLG-HETCOR $^{1}H-^{13}C$), which is consistent with the crystallographic data (i.e., two inequivalent water molecules).[37] Recently, ^{1}H NMR has also been used to analyze crystalline phases of the calcium oxalate minerals present in kidney stones:[37] it was demonstrated that T_2^* edited ^{1}H and $^{1}H-^{1}H$ double-quantum (DQ) NMR experiments can be used to separate the organic and mineral parts within stones, showing them to be more insightful than the routinely used IR spectroscopy.[37] Lastly, ^{13}C NMR (spin-1/2 nucleus of moderate receptivity, $\gamma = 6.7281 \times 10^7$ rad s^{-1} T^{-1}) studies on COM have shown that the NMR signature of this nucleus is particularly sensitive to temperature, as attested by the changes in the resolution of the four peaks belonging to the two inequivalent oxalate ions, and ^{13}C was further used to follow structural transformations from COT to COM.[36,41] A tentative assignment of all carbon signals was then proposed with the help of density functional theory (DFT) and gauge including projector augmented wave (GIPAW) calculations of NMR parameters.[36]

To date, XRD has been the main analytical tool used to follow the different temperature phase transitions of calcium oxalates:[11,12,21,24] for example, the LT to HT structural change was shown to induce the disappearance of two peaks at $2\theta \approx 30°$ in the XRD pattern (Co Kα radiation).[24] However, as mentioned before, the involvement of water in the formation of the oxalate crystal structures and the mechanisms of phase transitions are still unclear. Therefore, suitable tools to study these molecules within the structure are needed, and in this context, solid-state NMR studies of ^{17}O and ^2H nuclei naturally appear as an attractive approach. To the best of our knowledge, none of these two nuclei have been used before to study the structure of calcium oxalate phases by NMR despite the fact that both have been shown to potentially provide excellent insight into the local environment and dynamics of water molecules in hydrated minerals and other crystalline phases.[47,48,57,49−56] Yet, deuterium and oxygen-17 are quadrupolar nuclei (^{17}O is spin-5/2 and ^2H is spin-1, with $\gamma = -3.6264 \times 10^7$ and 4.1065×10^7 rad s^{-1} T^{-1}, respectively),

with very low natural abundances (0.037% for ^{17}O and 0.0115% for $^2H^{\perp}$),[58,59] making high-resolution NMR analysis "ineffective" under standard NMR acquisition conditions. Therefore, isotopic enrichment (i.e., in ^{17}O and ^2H) is essential to study them via high-resolution solid-state NMR spectroscopy.

The first part of this manuscript focuses on the development of a cost-effective and user-friendly isotopic enrichment protocol for labeling the ^{17}O and ^2H nuclei of the water molecules within the COM structure. Isotopic enrichment of water in hydrated minerals, so far, has mainly been achieved via a recrystallization process.[55−57,60] However, crystallization can be time-consuming and requires large quantities of labeled water, consequently being very expensive, particularly in the case of oxygen-17 due to the high cost of ^{17}O-labeled water (from 1800 to 2900 EUR for 1 mL of 90% oxygen-17 enriched H_2O as of publication date). In this manuscript, we decided to explore if mechanochemistry with mild milling conditions and involving microliter quantities of water could be used to achieve isotopic enrichment of water molecules within the COM structure without affecting the crystallinity of the starting material. Building upon our recent demonstration that mechanochemistry can be a very powerful technique for enriching in ^{17}O various inorganic materials and organic molecules,[61−66] we will demonstrate for the first time that ball-milling methods are also very well suited for the ^{17}O-labeling or deuteration of hydrated biomimetic minerals like calcium oxalates. Moreover, it will be shown how information on the actual enrichment mechanism of this mechanochemical labeling procedure can be obtained by using two complementary mass spectrometry methods (one bulk and one for the surface) and analyzing the isotopic compositions of COM phases with water molecules enriched in ^2H, ^{17}O, or ^{18}O (the latter being prepared for these mechanistic studies).

In the second part, this manuscript will present high-resolution ^{17}O and ^2H NMR analyses of COM, together with GIPAW DFT calculations of NMR parameters, to help explain the spectral features related to the two water molecules. Additional variable-temperature ^{17}O and ^2H NMR experiments will be shown, providing unprecedented insights into the dynamics of the water molecules within the COM structure, including during the LT to HT transition, and shedding light on the potential role of the water molecules in this transformation.

■ EXPERIMENTAL SECTION

Materials and Methods. *Reagents.* Calcium oxalate monohydrate (COM, $CaC_2O_4 \cdot H_2O$, 99%, Alfa Aesar), sodium oxalate ($Na_2C_2O_4$, 99%, Sigma-Aldrich), calcium chloride dihydrate ($CaCl_2 \cdot 2H_2O$, 99%, Sigma-Aldrich), $H_2^{17}O$ (~90% ^{17}O enrichment, CortecNet), $H_2^{18}O$ (99.3% ^{18}O enrichment, CortecNet), D_2O (≥99% ^2H enrichment, Sigma-Aldrich), and HPLC-grade water (Acros Organics) were used as received. COD was prepared as previously described in the literature[37,41] and stored under vacuum before any further use.

^{17}O, ^{18}O, and ^2H Isotopic Enrichment Procedures of COM Using Mechanochemistry. All milling experiments described here were carried out in a Retsch Mixer Mill MM400 apparatus operated at room temperature (22 ± 4 °C). Milling jars and beads were dried under vacuum prior to use. First, one polytetrafluoroethylene (PTFE) ball with a steel core (10 mm diameter) was placed in a 10 mL stainless steel grinding jar (with a screw-top lid). On top of the ball, nonlabeled

$CaC_2O_4 \cdot H_2O$ (60 mg, ~0.4 mmol, ~1 equiv) was added. Isotopically enriched water (7 μL, ~0.4 mmol, ~1 equiv) was then deposited to the reactor's wall. The jar was closed, sealed with parafilm, and subjected to grinding for 5 min in the mixer mill operated at 25 Hz. Although the exact change in temperature inside the jar during this milling process could not be measured, it is expected to be small under such conditions (less than ~25 °C).[67,68]

Three types of experiments were performed: (1) milling with the sample being collected directly after the reaction, abbreviated as COM-BM; (2) milling followed by an additional aging step, during which the sample was left in the closed grinding jar for 72 h at room temperature, abbreviated as COM-BM-AGED; and (3) milling with no PTFE ball and sample collection straight after the reaction, abbreviated as COM-SHAKE. The given abbreviations used herein were modified further in this manuscript by adding -^2H, -^{17}O, or -^{18}O at the end to indicate the enriched nuclei in the material (Scheme 1).

Scheme 1. Schematic Representation of the Mechanochemical Labeling Strategy Together with All Samples Prepared in This Study[a]
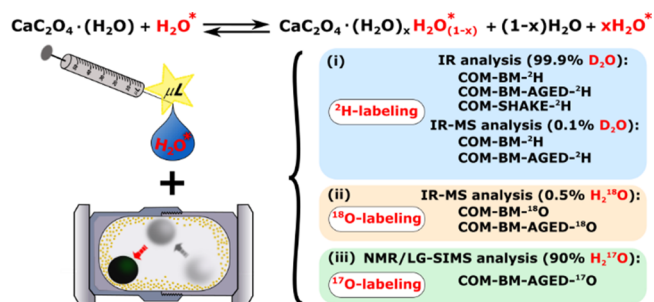
[a](i) Deuterium-enriched COM samples for IR (using 99.9% D_2O) and IR-MS (using 0.1% D_2O) analyses; (ii) ^{18}O-enriched COM samples for IR-MS analyses (using 0.5% $H_2^{18}O$); and (iii) ^{17}O-enriched COM sample for NMR and LG-SIMS analyses (using 90% $H_2^{17}O$).

Once all reactions were completed, the grinding jar was opened, and the white powder was recovered by gently scraping the edges of the reactor with a spatula (the ball was not scraped as no traces of material were observed on it). For COM-BM-AGED, the mass recovered was 54.0 ± 5.5 mg (n = 2, where n represents the number of independent experiments). For COM-BM and COM-SHAKE samples, an additional drying step (vacuum for ~5 min) was introduced straight after scraping the jar (as further detailed in the main text). The mass of the materials recovered was 54.6 ± 4.8 mg (n = 10) and 55.8 ± 4.7 mg (n = 5), respectively. All samples were stored in a parafilmed glass vial placed in a container with molecular sieves at −16 °C until further use. Prior to any characterization by IR, powder XRD (pXRD), SEM, IR-MS, and ^2H and ^{17}O NMR spectroscopy, samples were taken out of the freezer and left to thaw for 30 min.

Regarding the ^{18}O and ^2H enrichment procedures for IR-MS analyses, two isotopically diluted water solutions, enriched in ^{18}O or ^2H, were first prepared: $H_2^{18}O$ (99.3% ^{18}O) was diluted to ~0.5% and D_2O (≥99% ^2H) to ~0.1% in volume using HPLC-grade water. As described in the previous paragraphs, the COM precursor was then milled using either of these diluted waters. Three replicates per sample were prepared in

view of the analyses. Further information on the sample preparation for IR-MS and examples of calculating the exchange yield can be found in the Supporting Information (SI).

^{17}O-Labeling of COD by Mechanochemistry. The enrichment procedure was performed in the same way as it was described for COM in the previous section. Presynthesized and dried $CaC_2O_4 \cdot (2 + x)H_2O$ (60.7 mg, ∼0.35−0.37 mmol, ∼1 equiv) and 90% $H_2^{17}O$ (13 μL, ∼0.7 mmol, ∼2 equiv) were used and milled together for 5 min at 25 Hz. The white powder was recovered by gently scraping the jar and dried under a vacuum for ∼5 min to remove excess water; the mass of the final product was 54.5 mg. The sample was characterized using pXRD, IR spectroscopy, and ^{13}C NMR (Figure S3) and stored under an inert atmosphere when not in use.

Preparation of a Highly Deuterated COM Phase by Soaking. A highly deuterated COM phase (COM-SOAKED) was also prepared as part of this work by mixing $CaC_2O_4 \cdot H_2O$ (80.7 mg, 0.55 mmol) with D_2O (1 mL, 55.5 mmol, ∼100 equiv) in a 2 mL Eppendorf tube and leaving the suspension to set at room temperature for 3 days. Excess water was then removed by centrifuging the sample at 20,000 rpm for 10 min followed by drying under a vacuum for 6 h. The recovered mass was 69.4 mg. The material was further characterized by IR, pXRD, SEM, and ^{2}H solid-state NMR spectroscopy.

Characterization Techniques. Throughout this manuscript, deuterium nuclei are denoted as ^{2}H or D, and hence, the molecules/bonds in which they are engaged employ both notations.

This article deals with isotopic compositions and NMR chemical shifts, where both use by convention the δ notation. To differentiate between the two, here, when it is the isotopic composition that is discussed for oxygen and deuterium, the following notations are used: $\delta^{17}O$, $\delta^{18}O$, and δ^2H (expressed in per-mil (‰), as defined in the SI). In contrast, for the NMR chemical shifts for ^{17}O and ^{2}H, the following notations are used: $\delta(^{17}O)$ and $\delta(^2H)$ (expressed in ppm). Moreover, $\delta_{iso}(^{17}O)$ and $\delta_{iso}(^2H)$ notations refer to the corresponding isotropic chemical shifts.

General Characterization of the Samples. Infrared (IR) spectra were recorded on a Perkin Elmer Spectrum 2 FT-IR instrument (optical resolution of 0.5 cm^{-1}) in attenuated total reflectance (ATR) measurement mode (analyses in the 400−4000 cm^{-1} range, performed by averaging four acquisitions per sample).

pXRD analyses were performed on an X'Pert MPD diffractometer using Cu Kα_1 radiation (λ = 1.5406 Å) with the operating voltage and current maintained at 40 kV and 25 mA, respectively. Diffractograms were recorded between 5 and 60° in 2θ, with a step size of 0.017° (with a count time per step of ∼50 s).

SEM analyses were carried out on a Zeiss Evo HD15 scanning electron microscope equipped with an Oxford Instruments X-MaxN SDD 50 mm^2 EDXS detector. Before the SEM analyses, samples were deposited on a double-sided conducting carbon tape and then metallized with carbon.

Mass Spectrometry Analyses by IR-MS and LG-SIMS. Isotope Ratio Mass Spectrometry (IR-MS). Solid, powdered samples were analyzed at the AETE-ISO analytical platform of OSU OREME, at the University of Montpellier, using a Thermo DELTA V Plus gas source mass spectrometer connected to a TC/EA Elemental Analyzer. The instrumental precision was estimated to be ±3‰ and ± 0.4‰ for δ^2H and

$\delta^{18}O$, respectively, on solid samples. The samples were pyrolyzed at high temperatures (∼1400 °C) in the presence of a high excess of glassy carbon and converted to H_2 and CO gases. The molecular isotopic ratios of the gases produced (CO and H_2) were then measured by comparison with monitoring gases of known composition. The unenriched starting material of COM (COM-SM) and a benzoic acid chemical standard were also run at the beginning and in between measurements of isotopically enriched samples to ensure that there was no drift in the isotopic measurement as a result of improper pyrolysis. Further details and analysis of IR-MS results, including an example of the exchange yield calculations of both isotopes, are included in the SI.

Large Geometry Secondary Ion Mass Spectrometry (LG-SIMS). LG-SIMS analyses were carried out at the French national facility of the CRPG in Nancy on a CAMECA IMS 1280 HR ion microprobe. A ^{133}Cs$^+$ primary ion beam was used, and secondary ions were extracted, allowing ^{16}O, ^{17}O, and ^{18}O to be quantified simultaneously with a mass resolution of >2000. The instrument has been recently upgraded with high-sensitivity Faraday cups (FC 10^{12} Ω amplifiers).[69]

COM-SM and COM-BM-AGED-^{17}O samples were first pelletized and then embedded into indium alloy using a hydraulic press together with a standard reference sample, calcium carbonate. The embedded materials were sputtered with a thin layer of gold before being placed into the high vacuum chamber of the LG-SIMS instrument.

For each sample, average ^{17}O/^{16}O ratios were determined by analyzing a minimum of three different zones of the surface by performing 30 independent measurement cycles for each zone. The isotopic ratios reported herein (together with the standard deviations) correspond to an average over the different surface points that were analyzed, as shown in Table S5.

Solid-State NMR Experiments. Oxygen-17 NMR spectra were recorded at multiple magnetic fields (B_0 = 9.4, 14.1, 18.8, and 35.2 T) at different NMR facilities (ICGM in Montpellier, UCCS in Lille, and MagLab in Tallahassee). ^{17}O chemical shifts were referenced using tap water at 0.0 ppm (as commonly done in the literature), which corresponds to D_2O at −2.7 ppm (D_2O being the IUPAC recommended reference).[70] All detailed experimental conditions are summarized in Table S6.

Most of the ^{17}O NMR experiments were performed at 9.4 and 14.1 T on Varian VNMRS spectrometers (ICGM in Montpellier, France) using 3.2 mm HX or HXY probes operating at ^{17}O Larmor frequencies of 54.18 and 81.31 MHz, respectively. The corresponding ^{1}H Larmor frequencies were 399.68 and 599.82 MHz. Samples were spun at the magic angle (MAS, magic angle spinning) at a frequency of 18 kHz, and with the temperature regulated at 0 °C. The 1D ^{17}O MAS (Bloch decay) NMR experiments were performed using a 1.0 μs excitation pulse (corresponding to a 30° tilt angle on a liquid). The double-frequency sweep (DFS)[71] enhancement scheme was used in some of the experiments with a DFS pulse of 500 μs (RF of ∼10 kHz) and a sweep width between 80 and 200 kHz followed by an excitation pulse of 1.0 μs. SPINAL-64 ^{1}H decoupling was applied in all experiments.[72] Additional oxygen-17 T'_2 measurements were recorded using a Hahn echo experiment at 14.1 T with a 1.6 mm HXY Varian probe with a spinning frequency of 35 kHz with the temperature regulated at 0 °C. Echo delays were varied from 1 to 100 rotor periods, with π/2 and π pulse lengths of 1.0 and 2.0 μs, respectively.

At 18.8 T, ^{17}O MAS NMR spectra were recorded on a Bruker Avance NEO NMR spectrometer (UCCS in Lille, France) equipped with a 3.2 mm HX probe operating at frequencies of 108.46 and 800.12 MHz for ^{17}O and ^{1}H nuclei, respectively. The spinning frequency was controlled at 16 kHz, with the temperature regulated at 0 °C. The 1D ^{17}O MAS (Bloch decay) NMR experiment was performed using a 1.0 μs pulse for excitation (corresponding to a 22.5° tilt angle on a liquid). SPINAL-64 ^{1}H decoupling was applied in all experiments.

At 35.2 T, ^{17}O MAS NMR spectra were acquired using the SCH magnet[73] at the NHMFL (Tallahassee, FL, USA) on a Bruker Avance NEO NMR spectrometer equipped with a 3.2 mm single-resonance MAS probe operating at a ^{17}O frequency of 203.36 MHz. The spinning frequency was set to 18 kHz, and the temperature controlled at +10 °C. The 1D ^{17}O Hahn echo experiment was recorded using one rotor period with $\pi/2$ and π pulse lengths of 5.0 and 10.0 μs, respectively. No ^{1}H decoupling was applied for this experiment.

Static ^{2}H NMR experiments were recorded at 14.1 T on a Varian VNMRS spectrometer using a 3.2 mm HX probe operating at the ^{2}H Larmor frequency (92.08 MHz). Spectra were collected using a quadrupolar echo pulse sequence with a 90° pulse length of 2.25 μs and with delays of 30 μs between the pulses. Measurements were performed at different temperatures, ranging between −40 and +80 °C. ^{2}H chemical shifts were referenced with respect to D_2O at 4.6 ppm.

Temperature calibrations for NMR were performed using $Pb(NO_3)_2$.[74] All other NMR experimental details, such as the RF power used for decoupling, recycle delays, and the number of transients, are reported in Table S6.

Computational Studies. Geometry optimizations for COM and COD structures were carried out on the crystallographic data reported by Daudon *et al.*[31] and Tazzoli and Domeneghetti,[29] respectively. The missing protons for the COD were added to be consistent with the expected structure. Three compositions of the COD (general formula: $CaC_2O_4 \cdot (2 + x)H_2O$) were studied for the calculations, where the value of the "zeolitic" water (x) was set to 0.25, 0.375, and 0.5, to evaluate the potential effect on the calculated oxygen quadrupolar NMR parameters. Atomic positions were relaxed using the Vienna *ab initio* simulation package (VASP),[75,76] based on the Kohn−Sham DFT, and using a plane-wave pseudopotential approach with an energy cutoff of 400 eV and 4 × 2 × 3 and 2 × 2 × 3 k-point mesh for COM and COD structures, respectively. During the geometry optimization, unit cell parameters were kept fixed to ensure consistency between the experimental and optimized structures. Structural optimizations were performed in three steps: first, the proton positions were relaxed within the structure; then this optimized structure was used as a starting point to relax further the H and O positions of the water molecules; and finally, all atomic positions were relaxed. The calculations were carried out using 80 atoms per COM structure relaxation and 110, 113, and 116 for COD (for x with 0.25, 0.375, and 0.5, respectively).

NMR parameters were calculated for all structures using the QUANTUM-ESPRESSO code,[77] keeping the atomic positions equal to the values previously determined using VASP. The Perdew−Burke−Ernzerhof (PBE) generalized gradient approximation was used,[78] and the valence electrons were described by norm-conserving pseudopotentials[79] in the Kleinman−Bylander form.[80] The shielding tensor was computed using the

GIPAW approach.[81] The wave functions were expanded on a plane wave basis set with a kinetic energy cutoff of 80 Ry. The calculations were done using a k-space mesh density of ∼0.04 Å^{-1}.

The isotropic chemical shift δ_{iso} is defined as $\delta_{iso} \approx -(\sigma - \sigma_{ref})$, where σ is the isotropic shielding and σ_{ref} is the isotropic shielding for the same nucleus in a reference system.[82] A selection of different hydrates was used to establish a relevant reference chemical shift for ^{17}O (Table S7 and Figure S4). For these hydrates, the maximum deviation between experimental and DFT-calculated ^{17}O isotropic shifts was found to be 6 ppm. The quadrupolar moments (Q) used to calculate the C_Q were −2.558 and 0.286 fm^{-2} for ^{17}O and ^{2}H, respectively.[83]

Spectral Processing and Simulations. In this manuscript, we use the Herzfeld−Berger convention for chemical shift anisotropy parameters;[84] further terminology and definitions are given in the SI. All spectra that had been recorded on a Varian VNMRS console were converted to the TOPSPIN software (https://www.bruker.com/en.html) and further processed there. Exponential line broadening between 0 and 250 Hz was applied to the spectra, depending on the experiment. ^{17}O MAS NMR spectra were then fitted using DMFIT[85] or SOLA (available within TOPSPIN) software packages to extract quadrupolar and chemical shift parameters. The static ^{17}O NMR spectra were used to determine CSA parameters and Euler angles; corresponding values were extracted using the dual-field fitting mode available in DMFit.

^{2}H line-shapes, including 180° flips of water molecules, were simulated using the NMR-WEBLAB software (https://weblab2.mpip-mainz.mpg.de/weblab66/).[86] Further motionally averaged quadrupolar parameters with rotational vibrational distributions in addition to 180° flips were simulated using a MATLAB[87] script written by Z. Gan.

■ RESULTS AND DISCUSSION

Establishing an Enrichment Procedure for Water Molecules in Hydrated Biomimetic Minerals by Deuteration under Ball-Milling. Due to the very low natural abundance of ^{17}O and ^{2}H, isotopic enrichment is a necessary first step to be able to analyze the local environments of water molecules in hydrated minerals by high-resolution solid-state NMR spectroscopy. However, concerning oxygen-17, to the best of our knowledge, hydrates have mainly been isotopically enriched by recrystallization using ∼0.15 to 0.60 mL of $H_2^{17}O$-labeled water (for sample masses ranging between 80 and 300 mg),[55−57,60] and the enrichment procedures described typically took between 3 and 21 days. Therefore, we first focused on developing a more efficient and user-friendly isotopic enrichment strategy using mechanochemistry.

The first experiments were performed using D_2O to help establish an initial working protocol for the subsequent $H_2^{17}O$ enrichment of COM due to the lower cost of the deuterated water. The overall goal was to find a procedure enabling the exchange of a sufficient fraction of the nonlabeled water molecules of COM by labeled ones while using a minimal amount of enriched water during the reaction and without significantly changing the crystallinity of the initial phase or forming byproducts. The progress of the exchange was probed using infrared (IR) spectroscopy (Figure 2) since, upon deuteration, the intensity of the O−H stretching bands (3000−3500 cm^{-1}) decreases, while new bands appear in the
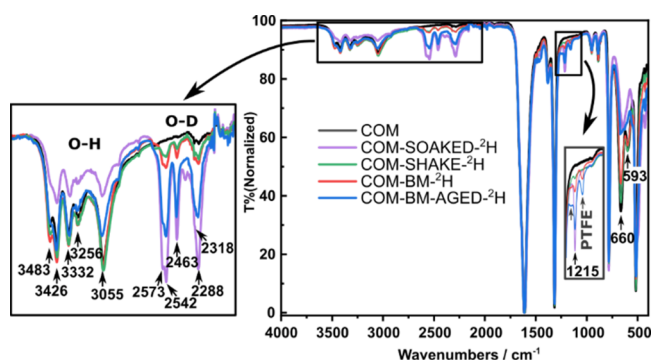
Figure 2. IR spectra of various COM samples as detailed in the figure legend with O−H and O−D stretching bands highlighted. The signals at 593 and 660 cm^{-1} correspond to libration modes of water, and that at 1215 cm^{-1} corresponds to the DOD bending mode. Signals highlighted with dark gray arrows (at 1156 and ∼1210 cm^{-1}) belong to PTFE,[92] which comes from the partial shedding of the PTFE ball during the milling.

2200−2600 cm^{-1} range due to O−D stretching vibrations of incorporated D$_2$O.[16,88]

First, a reference sample (COM-SOAKED-^{2}H) was prepared using large quantities of D$_2$O (∼100 equiv) to record a reference IR spectrum of the heavily deuterated sample and to identify all O−D stretching bands. The resulting IR spectrum is shown in Figure 2 in purple, with the five O−D stretching bands clearly visible in the 2200−2600 cm^{-1} range, mirroring the O−H stretching pattern. In addition, a weak band is observed at $\tilde{\nu}$ = 1215 cm^{-1} corresponding to a DOD bending mode, and the signals corresponding to libration modes of H$_2$O at $\tilde{\nu}$ = 591 and 659 cm^{-1} have decreased in intensity[33] (complete assignment of the IR spectrum provided in Figure S5 and Table S9).

Next, experiments were performed using much smaller quantities of D$_2$O (∼1 equiv with respect to COM, which corresponds to 7 μL of D$_2$O for 60 mg of the starting material). Here, to enable the efficient mixing of the COM precursor with the small volume of D$_2$O, experiments were carried out using mechanochemistry. This type of synthetic approach using small amounts of liquid (typically ∼0.1 μL/mg) during ball-milling is known as liquid-assisted grinding (LAG).[89] Here, enriched water was actually used to play the role of both a liquid grinding assistant and a reagent to introduce the isotopic label, in line with our previous work on isotopic labeling using ball-milling.[61−66] Three different experimental conditions were compared for the deuteration of COM. The first experiment adopted a very gentle approach: shaking for 5 min at 25 Hz without a milling ball (COM-SHAKE-^{2}H) to avoid affecting the crystallinity of the COM starting material. The second experiment was performed using the same quantities of reactants and same reaction conditions but with one PTFE milling ball added to the reactor (COM-BM-^{2}H). Both samples (COM-SHAKE-^{2}H and COM-BM-^{2}H) were dried under vacuum for 5 min after the reaction to remove excess surface water, as the presence of residual enriched/mobile water was evident from the IR spectra (Figure S6). Finally, using the aforementioned reaction conditions, a third experiment was performed in which the reaction mixture after 5 min of milling was then aged in a closed milling jar for 72 h (COM-BM-AGED-^{2}H). This process is referred to as accelerated aging[90,91] and was performed to investigate if exposure to the humidity of

enriched water in a sealed reactor could further increase the enrichment level. The resulting IR spectra are presented in Figure 2. All three samples show the expected O−D stretching bands in the 2200−2600 cm^{-1} range. COM-SHAKE-^{2}H and COM-BM-^{2}H show weaker O−D bands compared to the COM-BM-AGED-^{2}H sample. This result confirms that the aging step favors an increase in the number of enriched water molecules in the isolated COM phase.

Further, the crystallinity of deuterated COM samples was assessed by powder X-ray diffraction (Figure S7). No significant change in crystallinity was observed. Moreover, no diffraction peaks attesting to the formation of the other calcium oxalate hydrates (COD and COT) could be detected. Only a slight increase in the relative intensity of the diffraction peak at ∼24.5° was observed for the COM-BM-^{2}H and COM-BM-AGED-^{2}H samples. This small change may be related to the alteration in the particle morphology of the COM crystals upon grinding using the PTFE ball. This observation was further confirmed by examining the SEM images of the samples, where the overall particle size and shape and the agglomeration degree between particles were observed to vary after milling (Figure S8). Hence, overall, the labeling conditions used here are (i) mild enough to avoid any significant phase change of COM (or transformation into other hydrates) and yet (ii) sufficiently efficient to enable the deuteration of some of the crystallographic water molecules within the COM structure.

Quantification of the Mechanochemical Enrichment by Mass Spectrometry: Insight into the Labeling Mechanism. As mentioned above, the IR analyses of deuterated materials indicate a variation in the enrichment level between the samples presented. Therefore, to go one step further, the enrichment level was then estimated quantitatively using isotopic ratio mass spectrometry (IR-MS) and large-geometry secondary-ion mass spectrometry (LG-SIMS). In the former case, isotopic ratios are measured after pyrolysis of the sample (meaning that the ratios are representative of the average bulk composition of the samples). In contrast, in LG-SIMS, the isotopic composition within the first few atomic layers of the surface is analyzed after the bombardment of the surface by a primary ion beam.

In this study, we use two terms for describing and comparing the amount of enrichment within the samples prepared: enrichment yield and enrichment level. The enrichment yield depends on the given reaction conditions. Here, as the labeling reaction is reversible and performed by reacting ∼1 equiv of enriched water to ∼1 equiv of nonlabeled COM, the equilibrium is reached when 50% of the water molecules are exchanged within the COM material, which thus corresponds here to an enrichment yield of 100% regardless of the actual isotope enriched (when neglecting isotopic fractionation effects between bound water and remaining free water). Because of the type of labeling reaction involved, the *enrichment yield* will also be referred to as *exchange yield* in the rest of this manuscript. On the other hand, the enrichment level corresponds to the absolute percentage enrichment in ^{2}H, ^{17}O, or ^{18}O achieved within the sample (without considering the reaction mechanism).

IR-MS measurements were performed on freshly prepared samples on an instrument capable of resolving and quantifying minimal changes in ^{2}H/^{1}H and ^{18}O/^{16}O ratios (the ^{17}O/^{16}O ratios not being accurately measurable using the CO molecule as analyte). As IR-MS is optimized for the accurate

Scheme 2. Schematic Representation of Two Possible Pathways for the Isotopic Enrichment of Water Molecules in COM after the Ball-Milling Experiment
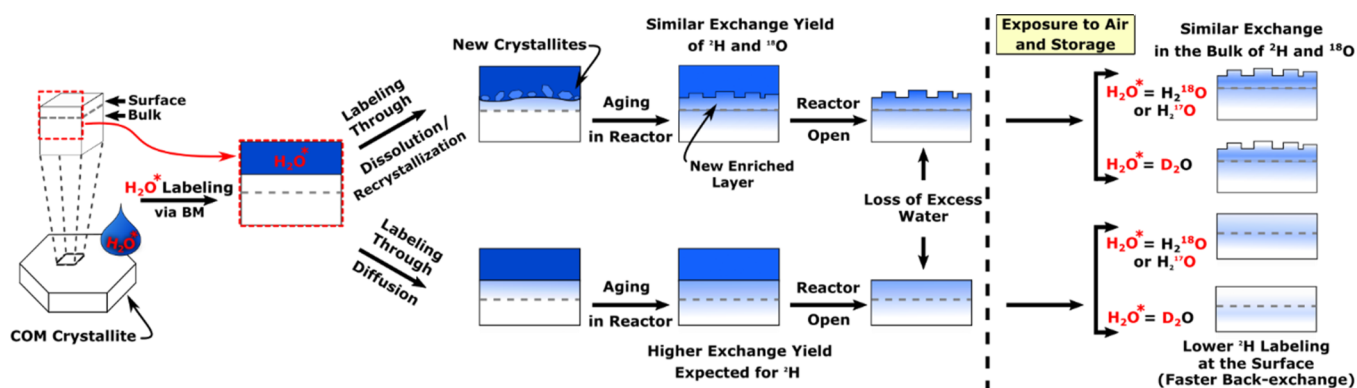
measurement of isotopic ratios close to natural abundances, especially in natural water, biological matrices, and minerals,[93] the COM enrichment procedure had to be adjusted by using enriched waters containing only ~0.1% D_2O or ~0.5% $H_2^{18}O$ in volume for the labeling to avoid any oversaturation of the detectors or contamination of the machine. Samples for IR-MS were prepared using the same ball-milling procedure as described previously, by reacting ~1 equiv of the diluted labeled water with ~1 equiv of COM, and isolated immediately or after aging.

IR-MS analyses on fresh samples showed that the exchange yields of water molecules were 7.8 ± 0.3 and 7.3 ± 0.1% for COM-BM-^{2}H and -^{18}O samples and 27.6 ± 1.0 and 34.1 ± 0.6% for COM-BM-AGED-^{2}H and -^{18}O samples, respectively (see the SI for further details and analysis of the IR-MS data). BM samples enriched using ^{18}O-labeled water showed very similar exchange yields to those enriched using ^{2}H-labeled water and slightly higher exchange yields after the aging step. The lack of preferential incorporation of deuterium suggests that the exchange of the enriched water molecules does not stem from a simple "diffusion" into the crystal structure (e.g., via hopping mechanisms for ^{2}H),[94] as a much higher incorporation rate of ^{2}H compared to ^{18}O would have been expected in this case even after 5 min of LAG. The absence of long-range H-bonded water networks within the COM structure actually supports the fact that such diffusion mechanisms are unlikely to be predominant: indeed, the water molecules are essentially associated as dimers in the lattice (Figure 1b). Moreover, subsequent ^{2}H NMR analyses also showed the absence of significant ^{2}H exchange between the two water sites even at high temperatures (as further detailed below). Hence, here, the relatively similar ^{2}H and ^{18}O exchange yields in COM-BM-^{2}H and -^{18}O samples suggest that the isotopic labeling in this material is rather arising from a mechanism enabling the exchange of the *full* water molecules, such as a rapid "dissolution−recrystallization" process occurring at the surface and interfaces of the crystallites during the 5 min of LAG, leading to the progressive formation of a COM phase incorporating enriched water molecules. This is further supported by the results shown for the aged samples where ~4 to 5 times higher exchange yield is detected, indicating that, in this case, the enrichment of the COM water molecules occurs more extensively within the bulk COM material, thanks to the prolonged "dissolution−recrystallization" processes in the sealed reactor (see Scheme 2).

The slightly lower ^{2}H-exchange yields after the aging step can be suspected to arise from the faster ^{1}H/^{2}H back-exchange within the *surface* layers of COM due to the much more rapid diffusion of the water protons inside/outside the surface of the materials (compared to the water oxygen atoms) when the sample is exposed to the ambient atmosphere (e.g., when the sample is recovered from the reactor or when other techniques are used to analyze it). The observation of a facilitated back-exchange for surface water could be in line with recent computational studies, which have shown that the COM surface contains defects where water molecules can easily penetrate.[42] Because back-exchange leads to a loss of isotopic enrichment, which can be problematic for NMR analyses, the deuterium-enriched samples were further used to evaluate the stability of the labeling in the COM material under different storage conditions. First, using IR spectroscopy, it was found that after 2 months of simple storage of COM-BM-^{2}H samples in a sealed vial in a freezer, the relative intensity of the O−D stretching bands in the 2200−2600 cm^{-1} range had decreased, while the O−H bands concomitantly had re-increased (Figure S9a), indicating a partial back-exchange of deuterated water molecules despite the low temperatures. Furthermore, IR-MS analyses of 2 week old COM-BM-^{2}H samples showed a decrease in the enrichment level from 7.8 ± 0.3 to 1.0 ± 0.1% (Table S2). All these results clearly show that proper storage is essential for maintaining the maximum enrichment of water molecules in the COM samples.

Considering that IR-MS analyses only provide an averaged isotopic composition of the materials, the studies presented above cannot inform on how the labeling within a COM crystallite varies from the surface to the core. Hence, as a first step toward probing in more detail the surface and subsurface isotopic composition of the enriched materials, LG-SIMS analyses were carried out. Here, measurements were performed on an instrument capable of resolving and quantifying the isotopic contents of the three stable isotopes of oxygen (^{16}O, ^{17}O, and ^{18}O). The COM-BM-AGED-^{17}O phase, which had been enriched using ~90% $H_2^{17}O$ water, was analyzed (Table S5). The resulting exchange yield was found to be 4.2 ± 1.5%, which is ~8 times lower compared to what had been measured by IR-MS. Such difference in the exchange yields can be related to the fact that IR-MS measures the isotopic composition of the whole sample, while LG-SIMS only measures the surface, and that partial loss of the enriched *surface* water molecules may have occurred prior to LG-SIMS. Indeed, LG-SIMS measurements were performed under ultra-
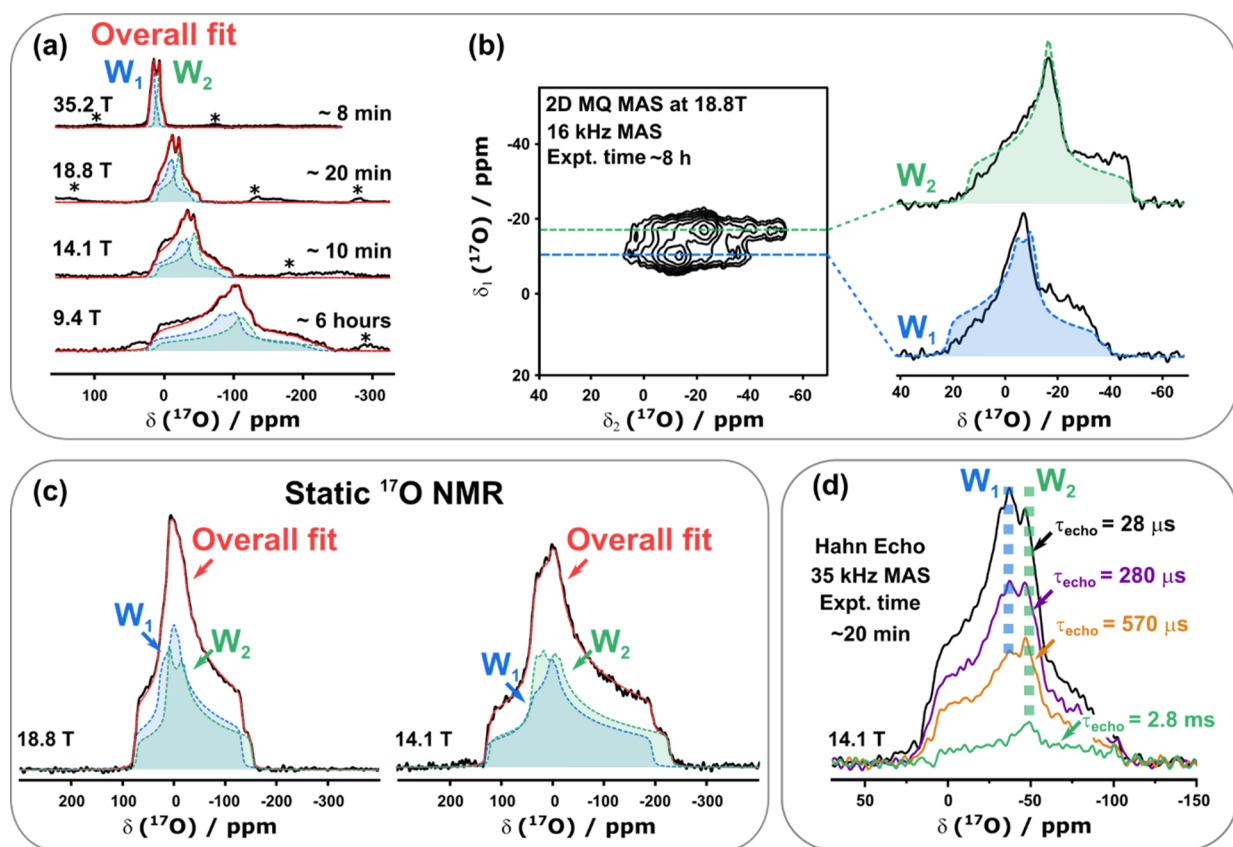
Figure 3. ^{17}O MAS NMR spectra of the COM-BM-AGED-^{17}O sample. (a) Experimental MAS spectra at 9.4, 14.1, 18.8, and 35.2 T (spinning side-bands highlighted with an asterisk) with simulated line-shapes shown in red. (b) 2D ^{17}O MQ MAS NMR spectrum at 18.8 T with two distinct water sites resolved and the extracted slices shown on the right (the overlaid green and blue line-shapes result from the multiple-field fitting of the 1D spectra). The resulting quadrupolar parameters are summarized in Table 1. Detailed experimental parameters are given in Table S6. (c) Static experimental ^{17}O NMR spectra recorded at 18.8 T (left) and 14.1 T (right), with simulated line-shapes shown in red. All resulting quadrupolar and CSA parameters are summarized in Table 1 and Table S10. The line-shape recorded at 18.8 T was also tentatively fitted without CSA using quadrupolar parameters reported in Table 1; the result is shown in Figure S12, clearly showing the effect of the CSA on the line-shape. (d) ^{17}O Hahn echo NMR experiments, performed under MAS at 14.1 T, show that the two sites have different T'_2 values.

high vacuum, and on a 4 week old sample, which, despite the precautions made in its preparation and storage, may have undergone surface back-exchange. This hypothesis was further confirmed by ^{17}O NMR analyses performed on the same sample ~6 weeks after its preparation (Figure S10): a decrease by only half in the ^{17}O NMR signal intensity was observed in the spectrum (and not by a factor of 8). Thus, overall, these measurements clearly confirm that the much larger decrease in exchange yield measured by LG-SIMS is indicative of the back-exchange processes occurring at the surface. More importantly, as it is a surface-sensitive technique, this shows how LG-SIMS is uniquely suited to probe changes in the surface composition of hydrated biomimetic materials and, as a consequence, the kinetics of back-exchange (which was beyond the scope of the present work).

Based on all the above analyses, it appears that (i) the water molecules in COM can be easily enriched in just 5 min in ^2H, ^{17}O, and ^{18}O using ball-milling and microliter quantities of isotopically labeled water without any significant change in the crystallinity of the material; (ii) a higher labeling level is readily achieved by a simple aging of the enriched material in a closed milling jar (with a maximum exchange yield of ~28−34% under the conditions tested here); and (iii) the storage conditions of the sample are essential to avoid any loss in isotopic label from back-exchange reactions with atmospheric

humidity at the sample surface. Considering the aforementioned points, a ^{17}O-enriched COM sample was prepared using ball-milling followed by an accelerated aging process as described previously (COM-BM-AGED-^{17}O). This sample was first characterized using IR and X-ray diffraction (Figures S7 and S11). The results of these analyses were consistent with those obtained for the deuterated sample. The exchange yield of the ^{17}O-enriched sample is assumed to be ~28−34% according to the IR-MS studies on similarly enriched ^2H and ^{18}O samples, which is suitable for high-resolution ^{17}O NMR analyses, as shown further.

Analysis of Local Water Environments Using High-Resolution ^{17}O NMR. Oxygen-17 NMR spectra of COM-BM-AGED-^{17}O were recorded at multiple fields (9.4, 14.1, 18.8, and 35.2 T) to extract quadrupolar parameters. The resulting one-dimensional (1D) spectra are shown in Figure 3a. All spectra were recorded in less than 20 min using a single pulse experiment except for the experiment performed at 9.4 T, which was recorded in 6 h due to the lower field strength and the poorer performance of the probe. The spectra at all fields showed well-defined line-shapes indicating the presence of crystalline water. Furthermore, a 2D MQMAS experiment allowed two water environments to be resolved (Figure 3b). This result is fully consistent with previous powder neutron diffraction[31] and IR[33,88] studies where two crystallographically

Table 1. Average Experimental ^{17}O NMR Parameters for the Two Water Molecules in COM, as Extracted from Measurements Performed at Different Fields[a]

experiment	δ_{iso} (ppm)	C_Q (MHz)	η_Q	Ω (ppm)	κ	assignment	magnetic field (T)
MAS	18.9 ± 1.0	6.5 ± 0.1	0.83 ± 0.02	-	-	W_1 site	9.4, 14.1, 18.8, and 35.2
	9.2 ± 1.1	6.5 ± 0.1	0.97 ± 0.02	-	-	W_2 site	
static	19 ± 4	6.4 ± 0.2	0.79 ± 0.03	53 ± 15	0.4 ± 0.1	W_1 site	14.1 and 18.8
	9 ± 3	6.3 ± 0.1	0.98 ± 0.02	47 ± 9	0.0 ± 0.2	W_2 site	

[a]See Figure 3 for experimental spectra and their fits and Table S6 for experimental acquisition parameters. Experimental C_Q values are given in absolute values.
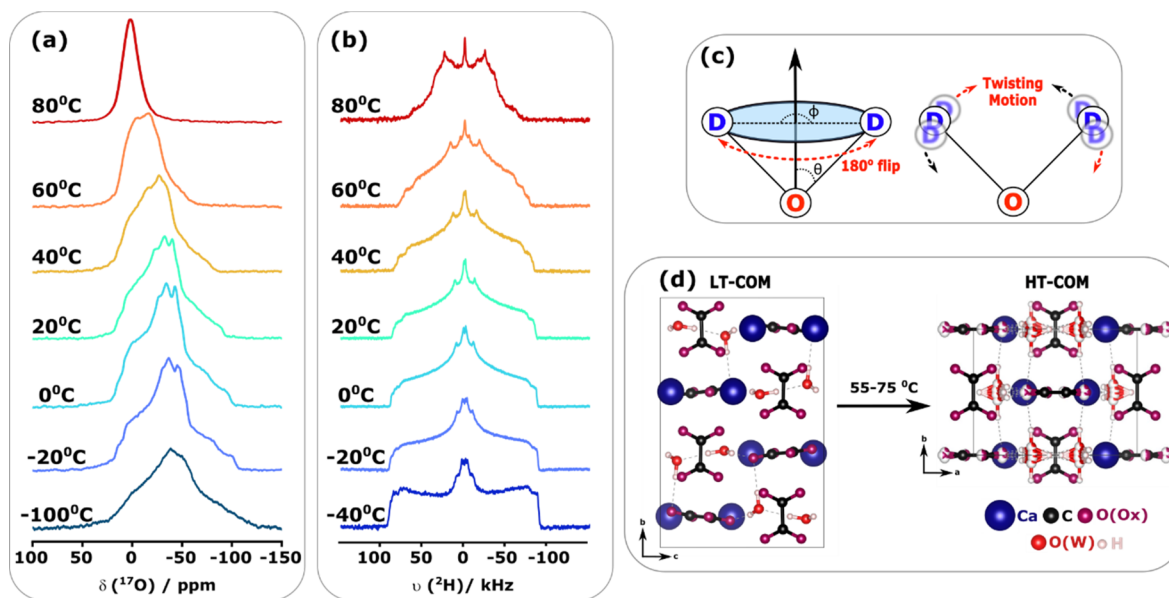

Figure 4. (a) Variable-temperature ^{17}O NMR measurements of COM-BM-AGED-^{17}O performed under MAS conditions at 14.1 T. (b) ^2H NMR spectra of COM-SOAKED-^2H recorded at different temperatures under static conditions. The soaked sample was chosen here rather than the BM phase due to its higher enrichment (see Figure 2), enabling one to obtain a better signal in a shorter time. Further ^2H and ^{17}O NMR experimental parameters are given in Table S6. (c) On the left: representation of the 180° jump (or C_2 symmetry jump) of the water molecule using a cone model. The cone angle is half of the D−O−D bond angle of the water molecule (denoted as θ), and the 180° flip is denoted with the angle φ. On the right: representation of the twisting motion of the deuterons in the water molecule. (d) Representation of the low-temperature (left) and high-temperature (right) structures of COM. Hydrogen bonding is highlighted with gray dashed lines. The previously proposed four possible orientations of the water oxygen atoms in the high-temperature structure are emphasized with partial white/red coloring; the latter structure was adapted from ref 44.

inequivalent water sites have been shown to be present within the COM structure.

The 2D ^{17}O MQMAS NMR spectrum was used to extract initial values of both water sites' isotropic chemical shifts and quadrupolar parameters. Using these values, the 1D ^{17}O MAS NMR spectra recorded at different fields were then further fitted. The resulting fits are presented in Figure 3a, with average experimental ^{17}O NMR parameters summarized in Table 1. All experiments were recorded under temperature control; however, it was not possible to obtain precisely the same temperature at the sample for the measurements at different fields. As a result, minor variations in the fitted quadrupolar parameters were observed. Average quadrupolar coupling constants (C_Q) were found to be 6.5 ± 0.1 MHz for both sites, with asymmetry values (η_Q) of 0.83 ± 0.02 and 0.97 ± 0.02 and isotropic chemical shifts (δ_{iso}) of 18.9 ± 1.0 and 9.2 ± 1.1 ppm, respectively. The measured values are consistent with other types of water molecules found in hydrated solids that have been previously studied by ^{17}O NMR where C_Q values ranged from 6.6 to 7.4 MHz, η_Q from 0.7 to 1.0,[55−57,60] and δ_{iso} covering a nearly 48 ppm range, i.e., from −17 ppm in

sodium perchlorate monohydrate[55] to 31.0 ppm in L-cysteine HCl monohydrate.[57]

Further, static experiments were performed to extract chemical shift anisotropy (CSA) parameters.[57,60] By examining closely the static ^{17}O NMR spectra recorded (Figure 3c), it is clear that there is a CSA contribution to the line-shape (see Figure S12 for simulations of static data with or without CSA at 18.8 T). Therefore, the span and skew (denoted as Ω and κ, respectively), as well as the Euler angles, were determined by fitting static ^{17}O line-shapes recorded at 14.1 and 18.8 T (Figure 3c) using as starting parameters the values taken from the GIPAW DFT calculations (see below and Table S11). All fitted parameters were then adjusted to find the best fit for both line-shapes. The resulting spans for the two sites were found to be equal to 53 ± 15 and 47 ± 9 ppm, with skews of 0.4 ± 0.1 and 0.0 ± 0.2, respectively, and with Euler angles as reported in Table S10. Although resulting CSA values still contain significant uncertainties (up to 30% in span), these results are consistent with those reported for the other experimentally fitted ^{17}O static spectra of hydrates reported in the literature where the span is observed to vary between 20 and 80 ppm, with error bars up to 30%.[55−57,60]

To help assign the two water sites, GIPAW calculations of NMR parameters of COM were performed. Atom positions were taken from the reported neutron diffraction structure[31] and progressively optimized. The results are summarized in Table S11, with additional computational details given in the SI. From the calculations, the site with the highest δ_{iso} corresponds to W_1 (20.39 ppm) and the lowest to W_2 (14.09 ppm). The other calculated ^{17}O NMR parameters are comparable to the experimental values, with C_Q being overestimated by ~20%. This difference can be explained by the fact that GIPAW calculates the NMR parameters without accounting for molecular motion, treating molecules and materials at 0 K. As a result, any motional averaging observed in experimental NMR would not be considered in the calculation. Previous studies of oxygen-17 for bound water in solids observed a similar discrepancy in the calculated C_Q parameters, and it was proposed that dynamics likely cause the differences.[57,60] Interestingly, a difference in T'_2 relaxation rates was observed here for both water molecules (Figure 3d). When performing a ^{17}O Hahn echo experiment, only the W_2 site was still observed after an echo delay of ~2.8 ms. More precisely, T'_2 values were estimated to be 0.336 ± 0.037 and 1.702 ± 0.087 ms for W_1 and W_2, respectively (Figure S13). For a quadrupolar nucleus like ^{17}O, these two contrasting relaxing rates may suggest that the dynamics of both sites are somewhat different. Thus, variable-temperature NMR experiments were performed to investigate the dynamics of water sites more closely.

Analysis of the Dynamics of Water Molecules in COM Using Variable-Temperature ^{17}O and ^2H NMR. As mentioned in the introduction, previous studies had shown that the COM lattice changes symmetry between 55 and 75 °C, and it had been proposed that this change is related to the appearance of a positional disorder on the water molecules and on some of the oxalate oxygen atoms.[24,44,45] Variable-temperature ^{17}O and ^2H NMR experiments were thus carried out to look into more detail at this phase transition from the water molecules' perspective (Figure 4a,b).

In the reported high-temperature structure of COM, to enable an $I2/m$ symmetry, the water molecules were proposed to statistically occupy four symmetry-related configurations, as shown in Figure 4d. Nevertheless, if water molecules were immobile, then the resulting line-shape of the ^{17}O nuclei at high temperatures should still maintain the same order of quadrupolar coupling and the same type of line-shape as shown at lower temperatures (i.e., below +40 °C, Figure 4a). However, a very different and much narrower line-shape is actually observed at high temperatures. This suggests that with increasing temperature (starting from +40 °C), the water molecules undergo rapid motions, changing their orientations within the lattice.

A closer analysis of the changes in ^{17}O line-shapes as a function of temperature was performed. First, by decreasing the temperature down to −100 °C (to try to freeze molecular motions), the experimental spectrum shows a broadening of the line-shape, where the C_Q of both sites increases by ~0.4 MHz, with little change observed for η_Q (Table S12 and Figure S14). However, the experimentally acquired C_Q values are not yet close to the calculated ones, suggesting that residual motion is still present at −100 °C. Conversely, with increasing temperature, the features of the quadrupolar line-shape gradually disappear between +40 and +60 °C, with further averaging observed at +80 °C. The symmetric signal at high

temperature is centered at 1.4 ppm, with a width at half-maximum of ~1400 Hz, which is both shifted and broader than what would have been detected for free "liquid" water.[95,96] The observed averaging of the quadrupolar line-shape and the apparent decrease in the C_Q values with increasing temperature are indicative of water molecules' motions within the COM lattice, where the local environments of oxygen atoms are affected by the movements of the surrounding H atoms, which result in rapid changes in the EFG (electric field gradient).[96] As expected, this temperature effect on the ^{17}O line-shape is reversible; i.e., after cooling the sample back to +20 °C, the initial quadrupolar line-shape of COM is recovered due to the reformation of the LT form (Figure S15).

Further analysis was performed on the COM-SOAKED-^2H sample using ^2H solid-state NMR to gain information on the local environment and dynamics of the water molecules.[47−52,97,98] Figure 4b shows the ^2H NMR quadrupolar echo spectra of COM-SOAKED-^2H recorded at 14.1 T in static mode between −40 and +80 °C. As in the case of ^{17}O NMR, changes in the recorded deuterium line-shapes are also observed over the whole temperature range. The resulting spectra cannot be fitted by only considering the DFT calculated quadrupolar parameters (C_Q and η_Q), as illustrated in Figure S16: molecular motions and their rate must be included to account for the different features in the recorded line-shapes.

At −40 °C, the spectrum is a result of water molecules undergoing a 180° jump around the bisector angle of the D−O−D bonds (Figure 4c, left). Using the bisector angles of the DFT-relaxed structure of COM (which are 52.2 and 54.2° for W_1 and W_2 water molecules, respectively) and the ^2H quadrupolar parameters calculated with the GIPAW method, a simulation of the resulting line-shapes as a function of the jump rate was performed for each water molecule (Figure S17). Based on the changes observed, it appears that in COM, at −40 °C, the jump rate of the water molecules is in an intermediate regime of ~10^6 s^{-1} (with quadrupolar parameters C_Q and η_Q between 200 and 210 kHz and 0.0 and 0.2, respectively).

At higher temperatures, the recorded spectra show that the water molecules enter into a fast exchange regime (>10^6 s^{-1}), as suggested by the simulation in Figure S17. The ^2H NMR spectra between −20 and +80 °C were fitted considering two water sites, leading to the motionally averaged deuterium quadrupolar parameters in Table S13 and Figure S18. Both C_Q and η_Q parameters for water sites revealed a trend, with a small progressive decrease by 18 kHz between −40 and +60 °C followed by a more significant change when transitioning to the HT-COM structure between +60 and +80 °C, where C_Q values were found to decrease further by ~20 kHz and η_Q by ~0.3 for both sites. Moreover, it was noted that while the averaged C_Q values for both sites were similar, the η_Q values were different for both sites and varied differently with temperature: for one site, the decrease in η_Q was ~0.23 between −40 and +60 °C, while for the other, it was ~0.09. Such changes cannot be accounted for by only considering 180° flips of the water molecules. The effect of a twisting vibration of the water molecules needs to be accounted for (Figure 4d, right). Simulations were carried out to see the effect of this motion on the quadrupolar parameters, where the amplitude of the motion was varied, and the effect of changes in the size of the bond angle for the water molecule was
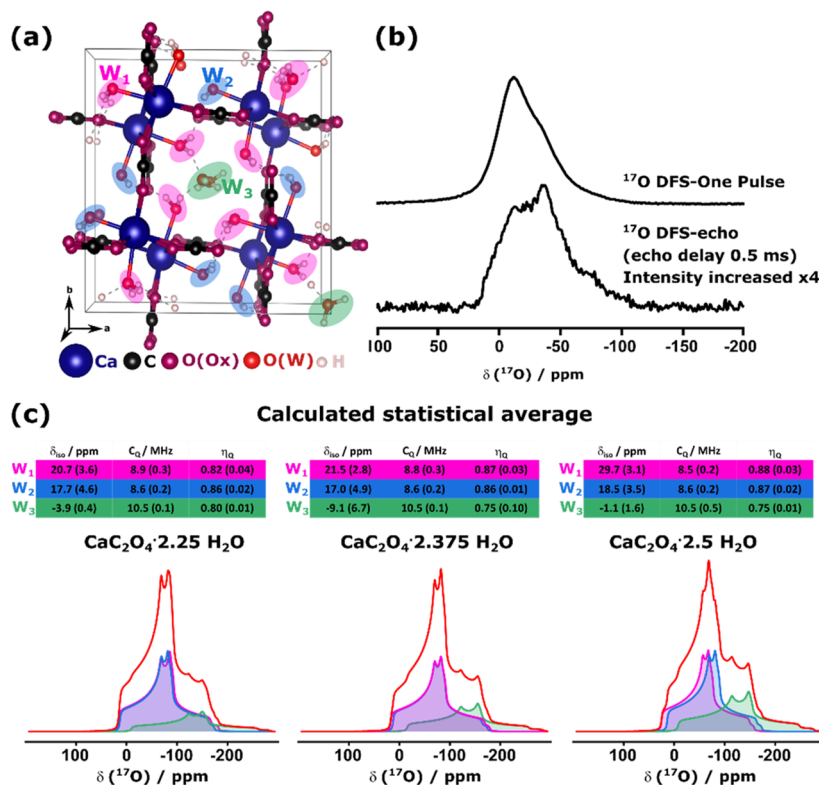
Figure 5. (a) Crystal structure of COD ($CaC_2O_4 \cdot (2.375)H_2O$) obtained after relaxing all atoms as described in the main text using the VASP software. The crystal structure by Tazzoli and Domeneghetti was used as a starting point (CCDC: 1293029).[29] Crystallographically equivalent water molecules are highlighted with purple, blue, and green ellipsoids. "Zeolitic" water is highlighted in green. The image of the crystal structure was produced using the VESTA software.[46] (b) 1D ^{17}O MAS NMR spectra of COD-BM-^{17}O recorded at 14.1 T using DFS single-pulse sequence (top) and the DFS-echo sequence with a 0.5 ms of echo delay (bottom; signal increased in intensity by a factor of 4 for a better comparison). Further NMR parameters are given in Table S6. (c) Simulated ^{17}O MAS NMR at 14.1 T line-shapes using the GIPAW DFT-calculated NMR parameters for three models of $CaC_2O_4 \cdot (2 + x)H_2O$, with x = 0.25, 0.375, and 0.5, with values from different types of water molecules averaged together. The integrated signal intensity of the "zeolitic" water was adjusted to match the overall water ratio within the COD structure. The content of "zeolitic" water (value of x) was varied to see the effect on the chemical shift and the quadrupolar parameters. The results of all calculations are summarized in Figure S20.

investigated (Figure S19). Including this motion can help rationalize the changes in averaged C_Q values extracted from the experimental spectra. The amplitude of the twisting motion was found to have a more significant effect on the apparent C_Q parameter, while the change in bond angle on the η_Q parameter. The quadrupolar parameters extracted from the static ^2H line-shapes show that one water site experiences a bigger variation in the bond angle compared to the other site (up to +60 °C), namely, the site where the bigger variation in the η_Q parameter is observed. Yet, both sites experience the same change in the averaged C_Q values, meaning that the amplitude of the twisting motion increases with temperature in the same manner for both sites. Lastly, measurements at +80 °C show that further transitioning to the HT-COM phase results in an increase in the bond angle for both sites and also in the twisting amplitude, as attested by a bigger change in the averaged quadrupolar parameters (Table S13).

The dynamics of the water molecules in COM and their importance in the phase change from the low- to the high-temperature forms could not have been simply derived from a careful analysis of their crystal structures or from previous solid-state NMR studies of water movements in other hydrated biomimetic minerals. Indeed, a great diversity of motions of water molecules within crystalline hydrates and water has been reported, mainly via ^2H NMR and, to a lesser extent, via ^{17}O

NMR.[47−54] While some structures have shown a "rigid" ^2H NMR line-shape (and hence the absence of movement) even at elevated temperatures (up to +100 °C), as in the case of $K_2C_2O_4 \cdot D_2O$,[99] in most cases, a characteristic line-shape that reflects the presence of molecular motions was observed (at rates $\geq 10^6$ s^{-1}). The most common movement reported for water molecules in crystalline hydrates has been a 180° flip of the water molecule about the C_2 symmetry axis,[49,50,98] as shown here for the LT-COM (at −40 °C). However, other motions, such as vibrations, have been previously shown to have an effect on the resulting apparent quadrupolar parameters, like a decrease in the experimentally measured C_Q of ^{17}O nuclei in $Ba(ClO_3)_2 \cdot H_2O$ due to the librational motion.[60] Here, we were able to show through variable-temperature ^2H NMR experiments and simulations that besides the C_2 symmetry jump, additional twisting motions take place, leading to changes in the appearance of the ^2H line-shape, and that variations in the averaged bond angle of water molecules can also have an effect on the resulting spectrum. Notably, the well-resolved ^2H powder patterns recorded between −40 and +80 °C reveal that two distinct water sites are still present, even in the HT-COM structure, with no measurable exchange occurring between both sites.

These ^2H and ^{17}O NMR results thus provide the first direct insight into the dynamics of the water molecules within the

different forms of COM. Overall, these variable-temperature studies clearly show that in addition to the changes in lattice symmetry and positional disorder occurring when transitioning from the LT to the HT structure, the water molecules are locally undergoing more pronounced molecular motions in the high-temperature form. To go even deeper in understanding the motions taking place in the high-temperature form of COM, further detailed variable-temperature studies and relaxation measurements of ^{2}H (including additional T_1, T'_2 relaxation experiments) would need to be performed, which are beyond the scope of the current work.

Outlook: Extension to the Study of Water Dynamics in Calcium Oxalate Dihydrate (COD). The present study has clearly shown that good ^{17}O-isotopic enrichment of the crystallographic water molecules of COM can be achieved using mechanochemistry under mild milling conditions and that, thanks to this labeling, information on the dynamics of the water molecules can be reached by NMR. Therefore, we further explored whether a similar approach could be used to enrich water molecules within the less stable COD phase.

The formula of COD is generally written as $CaC_2O_4 \cdot (2 + x)H_2O$, where x varies between 0 and 0.5 and corresponds to the so-called "zeolitic" water molecules (Figure 5a).[29,100−102] This phase is known to transform to the monohydrate phase over time under ambient atmospheric conditions, but a more rapid transformation is observed when the dihydrate is immersed in water.[12] Therefore, performing the isotopic enrichment of COD by immersion in enriched water would be highly expensive (due to the large quantities of enriched water used) and very likely to lead to the formation of an impure product (containing both COD and COM). Thus, proposing alternate strategies for labeling the water molecules appeared necessary to then be able to study the water dynamics.

Here, we tested the mechanochemical enrichment protocol presented above. The procedure was performed without the aging step to avoid unnecessary exposure to the water vapor, which could potentially transform dihydrate into monohydrate. The milled phase was first characterized using XRD, IR, and ^{13}C solid-state NMR (Figure S3), showing the purity of the COD product and the absence of formation of the monohydrate form. Although the recovered milled phase was dried under a vacuum after the enrichment step, potential small changes in the COD zeolitic water content x after milling were not studied at this stage. The resulting ^{17}O solid-state NMR spectrum was recorded (Figure 5b). As for COM, the data could be acquired in a short time ($\sim$4 h at 14.1 T), confirming the efficiency of this labeling strategy.

The ^{17}O NMR line-shape of COD shows fewer features than that of COM when comparing spectra recorded under similar acquisition conditions and at the same temperature. Yet, evidence of the presence of several different labeled water environments appeared clearly when comparing the spectra recorded using direct excitation (Figure 5b, top) or a Hahn echo experiment (Figure 5b, bottom). To further interpret the ^{17}O NMR data, GIPAW DFT calculations were performed on structural models of COD corresponding to different substitution levels of the zeolitic water ($x = 0.25$, 0.375, and 0.50). Spectral simulations of the calculated data were then performed in two ways: either by adding the contributions of each water molecule in the lattice (Figure S20e) or by preaveraging those corresponding to the same types of water sites (Figure 5c). In both cases, comparisons between the

simulated data and the experimentally recorded spectrum show that (i) more features are visible on the DFT-calculated spectra, while experimentally observed features are "smoothened", and (ii) the DFT-calculated quadrupolar parameters are once more overestimated as they were for the COM phase. These clearly suggest the presence of dynamics of the water molecules within the COD phase. To the best of our knowledge, this is not a point that has yet been studied for COD despite the fact that the water molecules are trapped within cavities, in which they would be prone to rapid reorientations as hinted by recently reported ^{1}H NMR data.[37] Hence, complementary variable-temperature experiments and ^{2}H NMR studies would need to be performed to shed further light on the nature of these movements, as detailed studies of water motions may help to better understand the phase transition from COD to COM.

■ CONCLUSIONS

In this work, a new approach for isotopically enriching water molecules in oxygen-17 and deuterium within hydrated biomimetic minerals has been presented via the use of mechanochemistry. The enrichment protocol used small quantities of labeled water ($\sim$7−13 μL for 60 mg of the starting material) and very short milling times ($\sim$5 min), making this method very efficient compared to conventional recrystallization techniques. This methodology was tested and optimized on the COM phase and then extended to the less stable COD form. In both cases, the characterizations performed using pXRD and IR spectroscopy showed no significant changes in the material after the milling procedure, with notably no loss in crystallinity of the mineral or formation of any byproducts. Hence, this labeling strategy should enable high-resolution NMR analyses to be performed on other hydrated biomaterials.

The efficiency of the enrichment protocol was extensively studied in the case of the COM phase using LG-SIMS and IR-MS methods. The average exchange yield of labeled water molecules was estimated to be $\sim$30% by IR-MS, while LG-SIMS provided the first insight into the surface isotopic composition of the COM crystallites. Here, we demonstrated how both analyses can complement one another by analyzing materials with water molecules enriched in ^{17}O, ^{18}O, or ^{2}H, thereby giving a better insight into the isotopic composition of the enriched materials and the labeling mechanism. In the case of COM, both LG-SIMS and IR-MS analyses showed that the enriched material experienced back-exchange of the water molecules at the surface upon exposure to the ambient atmosphere. Furthermore, results of IR-MS analyses showed that water molecules belonging to the bulk of the crystal structures also become enriched, most probably via a dissolution−recrystallization pathway occurring during the milling. From a more general perspective, such a high level of insight on the labeling mechanism is important for future developments in enrichment procedures based on mechanochemistry.

Thanks to the highly enriched phases prepared herein, the solid-state NMR analysis of ^{17}O and ^{2}H nuclei allowed us for the first time to gain structural and dynamic insights into the water molecules within the COM lattice. The ^{17}O NMR spectra could be recorded in a short time, enabling us to perform a 2D MQ MAS experiment in just a few hours, from which the two crystallographically inequivalent water sites could be resolved. Additional GIPAW DFT calculations of

NMR parameters permitted both water sites' assignments. More importantly, subsequent ^{17}O and ^2H variable-temperature studies enabled us to follow the dynamics of the water molecules when transitioning from the low- to the high-temperature structure. The NMR analysis provided insight into the movements of the water molecules within the COM structure. It was found that the water molecules are undergoing C_2 symmetry flips, where the jump rate of the water molecules is in an intermediate regime of $\sim 10^6$ s^{-1} below -40 °C and in the fast exchange regime ($>10^6$ s^{-1}) at higher temperatures. In addition to 180° flips, it was shown that with increasing temperature, a twisting motion comes into play, with its angular amplitude increasing up to $\sim 25°$, as shown by the ^2H line-shape of HT-COM. Furthermore, it was found by ^2H NMR that the water molecules are still inequivalent within the HT-COM structure and not exchanging their respective positions. In the previous analysis of these LT- to HT-COM transformations, which had been performed using X-ray diffraction and computational studies, it had been proposed that the water molecules within the HT-COM structure are occupying statistically disordered positions. Here, the variable-temperature ^{17}O and ^2H NMR analysis clearly shows that the water molecules are also undergoing fast molecular motions, as a result averaging the positions, with more pronounced movements and water distortions occurring in the HT form. Hence, overall, this study shows how solid-state NMR analyses of nuclei like ^{17}O and ^2H can be critical to the structural and the dynamical studies of the water molecules within hydrated biomimetic minerals like COM and may help shed light on the details of their phase transitions. Along the same line, preliminary ^{17}O NMR experiments of the COD phase also point to motions in the water molecules, which would deserve to be more thoroughly investigated in future work to better understand the poor stability of this phase and its transition into COM. As similar motions may also be occurring in other hydrated biominerals, we are currently looking into extending this labeling strategy to calcium pyrophosphates.

■ ASSOCIATED CONTENT

Ⓢ Supporting Information

The Supporting Information is available free of charge at https://pubs.acs.org/doi/10.1021/acs.jpcc.2c02070.

> Details on exchange yield estimation using IR-MS and LG-SIMS analysis; IR and pXRD results of various COM and COD samples described in this manuscript; NMR acquisition parameters used for all NMR experiments; conventions used for the definition of quadrupolar and CSA parameters; fitted static and MAS NMR data for oxygen-17 and static ^2H NMR data; experimental and calculated quadrupolar and CSA parameters of oxygen-17; details on GIPAW DFT calculations for ^{17}O and ^2H nuclei; ^2H NMR line-shapes calculated for C_2 symmetry jumps of the water molecules; and plots showing the effects of the motional averaging caused by a twisting motion on the apparent quadrupolar parameters of the water molecules (PDF)

■ AUTHOR INFORMATION

Corresponding Authors

Ieva Goldberga − ICGM, Univ Montpellier, CNRS, ENSCM, 34293 Montpellier, France; ● orcid.org/0000-0003-4284-3527; Email: ieva.goldberga@umontpellier.fr

Danielle Laurencin − ICGM, Univ Montpellier, CNRS, ENSCM, 34293 Montpellier, France; ● orcid.org/0000-0002-7445-0528; Email: danielle.laurencin@umontpellier.fr

Authors

Nicolas Patris − HydroSciences Montpellier, UMR 5151, CNRS, IRD, Université de Montpellier, 34090 Montpellier, France

Chia-Hsin Chen − ICGM, Univ Montpellier, CNRS, ENSCM, 34293 Montpellier, France; Present Address: Current affiliation: Johnson Matthey Technology Centre, Blount's Court, Sonning Common, Reading, RG4 9NH, United Kingdom; ● orcid.org/0000-0001-5151-1765

Emilie Thomassot − Université de Lorraine, CRPG, CNRS UMR 7358, 54500 Vandœuvre-lès-Nancy, France

Julien Trébosc − Université de Lille, CNRS, INRAE, Centrale Lille, Université d'Artois FR2638−IMEC−Institut Michel Eugène Chevreul, 59000 Lille, France

Ivan Hung − National High Magnetic Field Laboratory (NHMFL), Tallahassee, Florida 32310, United States; ● orcid.org/0000-0001-8916-739X

Zhehong Gan − National High Magnetic Field Laboratory (NHMFL), Tallahassee, Florida 32310, United States; ● orcid.org/0000-0002-9855-5113

Dorothée Berthomieu − ICGM, Univ Montpellier, CNRS, ENSCM, 34293 Montpellier, France

Thomas-Xavier Métro − IBMM, Univ Montpellier, CNRS, ENSCM, 34293 Montpellier, France; ● orcid.org/0000-0003-2280-3595

Christian Bonhomme − LCMCP, UMR 7574, Sorbonne Université, CNRS, 75005 Paris, France; ● orcid.org/0000-0003-0802-6961

Christel Gervais − LCMCP, UMR 7574, Sorbonne Université, CNRS, 75005 Paris, France

Complete contact information is available at:
https://pubs.acs.org/10.1021/acs.jpcc.2c02070

Author Contributions

The project was conducted by I.G. in close interaction with D.L. I.G. carried out all isotopic enrichment experiments, characterizations by IR, pXRD, and the vast majority of the solid-state NMR experiments. N.P. carried out IR-MS experiments and analysis of results, and E.T. conducted the LG-SIMS studies at the CRPG and performed multiple O-isotope calculations from raw data. I.H. and Z.G. performed experiments at 35.2 T (Tallahassee) and participated in the discussions and simulations of the ^2H NMR data. J.T. participated in the experiments recorded at 18.8 T (Lille). Some of the ^2H solid-state NMR experiments were carried out with the help of C.H.C. I.G. and C.G. carried out GIPAW DFT computations, and D.B. and D.L. participated in the discussions on computational results. T.X.M. participated in the discussions on mechanochemistry labeling reactions, while C.G. and C.B. participated in the discussions on solid-state NMR data. I.G .and D.L. wrote the initial draft of the manuscript, and all authors contributed to the final preparation of the article.

Notes

The authors declare no competing financial interest.

■ ADDITIONAL NOTE

$^{\perp}$There are two values reported for the natural abundance of the ^2H isotope, where 0.0115% corresponds to the terrestrial natural abundance of deuterium and 0.0156% corresponds to the mean ocean water composition (referred to as VSMOW). For isotopic composition calculations, the VSMOW value was used.

■ REFERENCES

(1) Echigo, T.; Kimata, M. Crystal Chemistry and Genesis of Organic Minerals: A Review of Oxalate and Polycyclic Aromatic Hydrocarbon Minerals. *Can. Mineral.* 2010, 48, 1329−1357.

(2) Dutton, M. V.; Evans, C. S. Oxalate Production by Fungi: Its Role in Pathogenicity and Ecology in the Soil Environment. *Can. J. Microbiol.* 1996, 42, 881−895.

(3) Giordani, P.; Modenesi, P.; Tretiach, M. Determinant Factors for the Formation of the Calcium Oxalate Minerals, Weddellite and Whewellite, on the Surface of Foliose Lichens. *Lichenologist* 2003, 35, 255−270.

(4) Coe, F. L.; Evan, A.; Worcester, E. Kidney Stone Disease. *J. Clin. Invest.* 2005, 115, 2598−2608.

(5) Khan, S. R.; Pearle, M. S.; Robertson, W. G.; Gambaro, G.; Canales, B. K.; Doizi, S.; Traxer, O.; Tiselius, H.-G. Kidney Stones. *Nat. Rev. Dis. Primers* 2016, 2, 16008.

(6) Daudon, M.; Dessombz, A.; Frochot, V.; Letavernier, E.; Haymann, J.-P.; Jungers, P.; Bazin, D. Comprehensive Morpho-Constitutional Analysis of Urinary Stones Improves Etiological Diagnosis and Therapeutic Strategy of Nephrolithiasis. *C. R. Chim.* 2016, 19, 1470−1491.

(7) Leavens, P. B. New Data on Whewellite. *Am. Mineral.* 1968, 53, 455−463.

(8) Cocco, G. La Struttura Della Whewellite. *Atti Acad. Naz. Lincei Cl. Sci. Fis. Mat. Nat.* 1961, 31, 292−298.

(9) Sterling, C. Crystal Structure Analysis of Weddellite, CaC$_2$O$_4$·(2+x)H$_2$O. *Acta Crystallogr.* 1965, 18, 917−921.

(10) Deganello, S.; Kampf, A. R.; Moore, P. B. The Crystal Structure of Calcium Oxalate Trihydrate: Ca(H$_2$O)$_3$(C$_2$O$_4$). *Am. Mineral.* 1981, 66, 859−865.

(11) Conti, C.; Brambilla, L.; Colombo, C.; Dellasega, D.; Gatta, G. D.; Realini, M.; Zerbi, G. Stability and Transformation Mechanism of Weddellite Nanocrystals Studied by X-Ray Diffraction and Infrared Spectroscopy. *Phys. Chem. Chem. Phys.* 2010, 12, 14560.

(12) Conti, C.; Casati, M.; Colombo, C.; Realini, M.; Brambilla, L.; Zerbi, G. Phase Transformation of Calcium Oxalate Dihydrate−Monohydrate: Effects of Relative Humidity and New Spectroscopic Data. *Spectrochim. Acta, Part A* 2014, 128, 413−419.

(13) Tomažič, B.; Nancollas, G. H. The Kinetics of Dissolution of Calcium Oxalate Hydrates. *J. Cryst. Growth* 1979, 46, 355−361.

(14) Daudon, M.; Letavernier, E.; Frochot, V.; Haymann, J.-P.; Bazin, D.; Jungers, P. Respective Influence of Calcium and Oxalate Urine Concentration on the Formation of Calcium Oxalate Monohydrate or Dihydrate Crystals. *C. R. Chim.* 2016, 19, 1504−1513.

(15) Ruiz-Agudo, E.; Burgos-Cara, A.; Ruiz-Agudo, C.; Ibañez-Velasco, A.; Cölfen, H.; Rodriguez-Navarro, C. A Non-Classical View on Calcium Oxalate Precipitation and the Role of Citrate. *Nat. Commun.* 2017, 8, 768.

(16) Gehl, A.; Dietzsch, M.; Mondeshki, M.; Bach, S.; Häger, T.; Panthöfer, M.; Barton, B.; Kolb, U.; Tremel, W. Anhydrous Amorphous Calcium Oxalate Nanoparticles from Ionic Liquids: Stable Crystallization Intermediates in the Formation of Whewellite. *Chem. - Eur. J.* 2015, 21, 18192−18201.

(17) Zhang, J.; Wang, L.; Zhang, W.; Putnis, C. V. Role of Hyperoxaluria/Hypercalciuria in Controlling the Hydrate Phase Selection of Pathological Calcium Oxalate Mineralization. *Cryst. Growth Des.* 2021, 21, 683−691.

(18) Ihli, J.; Wang, Y.-W.; Cantaert, B.; Kim, Y.-Y.; Green, D. C.; Bomans, P. H. H.; Sommerdijk, N. A. J. M.; Meldrum, F. C. Precipitation of Amorphous Calcium Oxalate in Aqueous Solution. *Chem. Mater.* 2015, 27, 3999−4007.

(19) Hajir, M.; Graf, R.; Tremel, W. Stable Amorphous Calcium Oxalate: Synthesis and Potential Intermediate in Biomineralization. *Chem. Commun.* 2014, 50, 6534−6536.

(20) Sherer, B. A.; Chen, L.; Kang, M.; Shimotake, A. R.; Wiener, S. V.; Chi, T.; Stoller, M. L.; Ho, S. P. A Continuum of Mineralization from Human Renal Pyramid to Stones on Stems. *Acta Biomater.* 2018, 71, 72−85.

(21) Hochrein, O.; Thomas, A.; Kniep, R. Revealing the Crystal Structure of Anhydrous Calcium Oxalate, Ca[C$_2$O$_4$], by a Combination of Atomistic Simulation and Rietveld Refinement. *Z. Anorg. Allg. Chem.* 2008, 634, 1826−1829.

(22) Zhang, D.; Li, S.; Zhang, Z.; Li, N.; Yuan, X.; Jia, Z.; Yang, J. Urinary Stone Composition Analysis and Clinical Characterization of 1520 Patients in Central China. *Sci. Rep.* 2021, 11, 6467.

(23) Daudon, M. Épidémiologie Actuelle de La Lithiase Rénale En France. *Ann. Urol. (Paris).* 2005, 39, 209−231.

(24) Izatulina, A. R.; Gurzhiy, V. V.; Krzhizhanovskaya, M. G.; Kuz'mina, M. A.; Leoni, M.; Frank-Kamenetskaya, O. V. Hydrated Calcium Oxalates: Crystal Structures, Thermal Stability, and Phase Evolution. *Cryst. Growth Des.* 2018, 18, 5465−5478.

(25) Wiedemann, G.; Bayer, G. Kinetics of the Formation of Whewellite and Weddelite by Displacement Reactions. *J. Therm. Anal.* 1988, 33, 707−718.

(26) Frost, R. L.; Weier, M. L. Thermal Treatment of Weddellite—a Raman and Infrared Emission Spectroscopic Study. *Thermochim. Acta* 2003, 406, 221−232.

(27) Daudon, M.; Letavernier, E.; Weil, R.; Véron, E.; Matzen, G.; André, G.; Bazin, D. Type 2 Diabetes and Uric Acid Stones: A Powder Neutron Diffraction Investigation. *C. R. Chim.* 2016, 19, 1527−1534.

(28) Echigo, T.; Kimata, M.; Kyono, A.; Shimizu, M.; Hatta, T. Re-Investigation of the Crystal Structure of Whewellite [Ca(C$_2$O$_4$)·H$_2$O] and the Dehydration Mechanism of Caoxite [Ca(C$_2$O$_4$)·3H$_2$O]. *Mineral. Mag.* 2005, 69, 77−88.

(29) Tazzoli, V.; Domeneghetti, C. The Crystal Structures of Whewellite and Weddellite: Re-Examination and Comparison. *Am. Mineral.* 1980, 65, 327−334.

(30) Gay, C.; Letavernier, E.; Verpont, M.-C.; Walls, M.; Bazin, D.; Daudon, M.; Nassif, N.; Stéphan, O.; de Frutos, M. Nanoscale

Analysis of Randall's Plaques by Electron Energy Loss Spectromicroscopy: Insight in Early Biomineral Formation in Human Kidney. *ACS Nano* **2020**, *14*, 1823−1836.

(31) Daudon, M.; Bazin, D.; André, G.; Jungers, P.; Cousson, A.; Chevallier, P.; Véron, E.; Matzen, G. Examination of Whewellite Kidney Stones by Scanning Electron Microscopy and Powder Neutron Diffraction Techniques. *J. Appl. Crystallogr.* **2009**, *42*, 109−115.

(32) Petit, I.; Belletti, G. D.; Debroise, T.; Llansola-Portoles, M. J.; Lucas, I. T.; Leroy, C.; Bonhomme, C.; Bonhomme-Coury, L.; Bazin, D.; Daudon, M.; et al. Vibrational Signatures of Calcium Oxalate Polyhydrates. *ChemistrySelect* **2018**, *3*, 8801−8812.

(33) Shippey, T. A. Vibrational Studies of Calcium Oxalate Monohydrate (Whewellite) and Anhydrous Phase of Calcium Oxalate. *J. Mol. Struct.* **1980**, *63*, 157−166.

(34) Bazin, D.; Leroy, C.; Tielens, F.; Bonhomme, C.; Bonhomme-Coury, L.; Damay, F.; Le Denmat, D.; Sadoine, J.; Rode, J.; Frochot, V.; et al. Hyperoxaluria Is Related to Whewellite and Hypercalciuria to Weddellite: What Happens When Crystalline Conversion Occurs? *C. R. Chim.* **2016**, *19*, 1492−1503.

(35) Petrov, I.; Šoptrajanov, B. Infrared Spectrum of Whewellite. *Spectrochim. Acta Part* **1975**, *31*, 309−316.

(36) Colas, H.; Bonhomme-Coury, L.; Diogo, C. C.; Tielens, F.; Babonneau, F.; Gervais, C.; Bazin, D.; Laurencin, D.; Smith, M. E.; Hanna, J. V.; et al. Whewellite, $CaC_2O_4 \cdot H_2O$: Structural Study by a Combined NMR, Crystallography and Modelling Approach. *CrystEngComm* **2013**, *15*, 8840.

(37) Leroy, C.; Bonhomme-Coury, L.; Gervais, C.; Tielens, F.; Babonneau, F.; Daudon, M.; Bazin, D.; Letavernier, E.; Laurencin, D.; Iuga, D.; et al. A Novel Multinuclear Solid-State NMR Approach for the Characterization of Kidney Stones. *Magn. Reson.* **2021**, *2*, 653−671.

(38) Bowers, G. M.; Kirkpatrick, R. J. Natural Abundance ^{43}Ca NMR as a Tool for Exploring Calcium Biomineralization: Renal Stone Formation and Growth. *Cryst. Growth Des.* **2011**, *11*, 5188−5191.

(39) Bonhomme, C.; Wang, X.; Hung, I.; Gan, Z.; Gervais, C.; Sassoye, C.; Rimsza, J.; Du, J.; Smith, M. E.; Hanna, J. V.; et al. Pushing the Limits of Sensitivity and Resolution for Natural Abundance ^{43}Ca NMR Using Ultra-High Magnetic Field (35.2 T). *Chem. Commun.* **2018**, *54*, 9591−9594.

(40) Bak, M.; Jens, K. T.; Hans, J. J.; Steffen, E. P.; Torben, E. P.; Neils, C. N. Solid-State ^{13}C and ^{31}P NMR Analysis of Urinary Stones. *J. Urol.* **2000**, *164*, 856−863.

(41) Leroy, C. Oxalates de Calcium et Hydroxyapatite: Des Matériaux Synthétiques et Naturels Étudiés Par Techniques RMN et DNP. Doctoral dissertation, Université Pierre et Marie Curie - Paris VI, 2016.

(42) Debroise, T.; Sedzik, T.; Vekeman, J.; Su, Y.; Bonhomme, C.; Tielens, F. Morphology of Calcium Oxalate Polyhydrates: A Quantum Chemical and Computational Study. *Cryst. Growth Des.* **2020**, *20*, 3807−3815.

(43) Zhao, W.; Sharma, N.; Jones, F.; Raiteri, P.; Gale, J. D.; Demichelis, R. Anhydrous Calcium Oxalate Polymorphism: A Combined Computational and Synchrotron X-Ray Diffraction Study. *Cryst. Growth Des.* **2016**, *16*, 5954−5965.

(44) Shepelenko, M.; Feldman, Y.; Leiserowitz, L.; Kronik, L. Order and Disorder in Calcium Oxalate Monohydrate: Insights from First-Principles Calculations. *Cryst. Growth Des.* **2020**, *20*, 858−865.

(45) Deganello, S. The Structure of Whewellite, $CaC_2O_4 \cdot H_2O$, at 328K. *Acta Crystallogr.* **1981**, *B37*, 826−829.

(46) Momma, K.; Izumi, F. VESTA 3 for Three-Dimensional Visualization of Crystal, Volumetric and Morphology Data. *J. Appl. Crystallogr.* **2011**, *44*, 1272−1276.

(47) Long, J. R.; Ebelhäuser, R.; Griffin, R. G. ^2H NMR Line Shapes and Spin−Lattice Relaxation in $Ba(ClO_3)_2 \cdot 2H_2O$. *J. Phys. Chem. A* **1997**, *101*, 988−994.

(48) O'Hare, B.; Grutzeck, M. W.; Kim, S. H.; Asay, D. B.; Benesi, A. J. Solid State Water Motions Revealed by Deuterium Relaxation in

^2H_2O-Synthesized Kanemite and ^2H_2O-Hydrated Na^+-Zeolite A. *J. Magn. Reson.* **2008**, *195*, 85−102.

(49) Tobar, C.; Cordova, R.; Solomon, T.; Palombo, K.; Olivares, G.; Helston, J.; Luo, W.; Cizmeciyan, D.; Benesi, A. Water Dynamics in Deuterated Gypsum, $CaSO_4 \cdot 2D_2O$, Investigated by Solid State Deuterium NMR. *J. Magn. Reson.* **2020**, *310*, No. 106640.

(50) Kolokolov, D. I.; Glaznev, I. S.; Aristov, Y. I.; Stepanov, A. G.; Jobic, H. Water Dynamics in Bulk and Dispersed in Silica $CaCl_2$ Hydrates Studied by ^2H NMR. *J. Phys. Chem. C* **2008**, *112*, 12853−12860.

(51) Benesi, A. J.; Grutzeck, M. W.; O'Hare, B.; Phair, J. W. Room Temperature Solid Surface Water with Tetrahedral Jumps of ^2H Nuclei Detected in ^2H_2O-Hydrated Porous Silicates. *J. Phys. Chem. B* **2004**, *108*, 17783−17790.

(52) Wittebort, R. J.; Usha, M. G.; Ruben, D. J.; Wemmer, D. E.; Pines, A. Observation of Molecular Reorientation in Ice by Proton and Deuterium Magnetic Resonance. *J. Am. Chem. Soc.* **1988**, *110*, 5668−5671.

(53) Takeda, S.; Gotoh, Y.; Maruta, G.; Takahara, S.; Kittaka, S. Restricted Rotational Motion of Interlayer Water Molecules in Vanadium Pentoxide Hydrate, $V_2O_5 \cdot D_2O$, as Studied by Deuterium NMR. *Z. Naturforsch. A* **2002**, *57*, 419−424.

(54) Bowers, G. M.; Singer, J. W.; Bish, D. L.; Kirkpatrick, R. J. Alkali Metal and H_2O Dynamics at the Smectite/Water Interface. *J. Phys. Chem. C* **2011**, *115*, 23395−23407.

(55) Nour, S.; Widdifield, C. M.; Kobera, L.; Burgess, K. M. N.; Errulat, D.; Terskikh, V. V.; Bryce, D. L. Oxygen-17 NMR Spectroscopy of Water Molecules in Solid Hydrates. *Can. J. Chem.* **2016**, *94*, 189−197.

(56) Keeler, E. G.; Michaelis, V. K.; Wilson, C. B.; Hung, I.; Wang, X.; Gan, Z.; Griffin, R. G. High-Resolution ^{17}O NMR Spectroscopy of Structural Water. *J. Phys. Chem. B* **2019**, *123*, 3061−3067.

(57) Michaelis, V. K.; Keeler, E. G.; Ong, T.-C.; Craigen, K. N.; Penzel, S.; Wren, J. E. C.; Kroeker, S.; Griffin, R. G. Structural Insights into Bound Water in Crystalline Amino Acids: Experimental and Theoretical ^{17}O NMR. *J. Phys. Chem. B* **2015**, *119*, 8024−8036.

(58) de Laeter, J. R.; Böhlke, J. K.; De Bièvre, P.; Hidaka, H.; Peiser, H. S.; Rosman, K. J. R.; Taylor, P. D. P. Atomic Weights of the Elements. Review 2000 (IUPAC Technical Report). *Pure Appl. Chem.* **2003**, *75*, 683−800.

(59) Hagemann, R.; Nief, G.; Roth, E. Absolute Isotopic Scale for Deuterium Analysis of Natural Waters. Absolute D/H Ratio for SMOW. *Tellus* **1970**, *22*, 712−715.

(60) Keeler, E. G.; Michaelis, V. K.; Griffin, R. G. ^{17}O NMR Investigation of Water Structure and Dynamics. *J. Phys. Chem. B* **2016**, *120*, 7851−7858.

(61) Métro, T.-X.; Gervais, C.; Martinez, A.; Bonhomme, C.; Laurencin, D. Unleashing the Potential of ^{17}O NMR Spectroscopy Using Mechanochemistry. *Angew. Chem., Int. Ed.* **2017**, *56*, 6803−6807.

(62) Chen, C.-H.; Mentink-Vigier, F.; Trébosc, J.; Goldberga, I.; Gaveau, P.; Thomassot, E.; Iuga, D.; Smith, M. E.; Chen, K.; Gan, Z.; et al. Labeling and Probing the Silica Surface Using Mechanochemistry and ^{17}O NMR Spectroscopy. *Chem. − A Eur. J.* **2021**, *27*, 12574−12588.

(63) Špačková, J.; Fabra, C.; Mittelette, S.; Gaillard, E.; Chen, C.-H.; Cazals, G.; Lebrun, A.; Sene, S.; Berthomieu, D.; Chen, K.; et al. Unveiling the Structure and Reactivity of Fatty-Acid Based (Nano)-Materials Thanks to Efficient and Scalable ^{17}O and ^{18}O-Isotopic Labeling Schemes. *J. Am. Chem. Soc.* **2020**, *142*, 21068−21081.

(64) Chen, C.-H.; Gaillard, E.; Mentink-Vigier, F.; Chen, K.; Gan, Z.; Gaveau, P.; Rebière, B.; Berthelot, R.; Florian, P.; Bonhomme, C.; et al. Direct ^{17}O Isotopic Labeling of Oxides Using Mechanochemistry. *Inorg. Chem.* **2020**, *59*, 13050−13066.

(65) Špačková, J.; Fabra, C.; Cazals, G.; Hubert-Roux, M.; Schmitz-Afonso, I.; Goldberga, I.; Berthomieu, D.; Lebrun, A.; Métro, T.-X.; Laurencin, D. Cost-Efficient and User-Friendly ^{17}O/ ^{18}O Labeling Procedures of Fatty Acids Using Mechanochemistry. *Chem. Commun.* **2021**, *57*, 6812−6815.

(66) Chen, C.-H.; Goldberga, I.; Gaveau, P.; Mittelette, S.; Špačková, J.; Mullen, C.; Petit, I.; Métro, T.; Alonso, B.; Gervais, C.; et al. Looking into the Dynamics of Molecular Crystals of Ibuprofen and Terephthalic Acid Using ^{17}O and ^{2}H Nuclear Magnetic Resonance Analyses. *Magn. Reson. Chem.* 2021, 59, 975−990.

(67) Kulla, H.; Wilke, M.; Fischer, F.; Röllig, M.; Maierhofer, C.; Emmerling, F. Warming up for Mechanosynthesis - Temperature Development in Ball Mills during Synthesis. *Chem. Commun.* 2017, 53, 1664−1667.

(68) Leroy, C.; Mittelette, S.; Félix, G.; Fabregue, N.; Špačková, J.; Gaveau, P.; Métro, T.-X.; Laurencin, D. Operando Acoustic Analysis: A Valuable Method for Investigating Reaction Mechanisms in Mechanochemistry. *Chem. Sci.* 2022, 6328−6334.

(69) Bouden, N.; Villeneuve, J.; Marrocchi, Y.; Deloule, E.; Füri, E.; Gurenko, A.; Piani, L.; Thomassot, E.; Peres, P.; Fernandes, F. Triple Oxygen Isotope Measurements by Multi-Collector Secondary Ion Mass Spectrometry. *Front. Earth Sci.* 2021, 8, 1−9.

(70) Harris, R. K.; Becker, E. D.; Cabral De Menezes, S. M.; Granger, P.; Hoffman, R. E.; Zilm, K. W. Further Conventions for NMR Shielding and Chemical Shifts (IUPAC Recommendations 2008). *Pure Appl. Chem.* 2008, 80, 59−84.

(71) Kentgens, A. P. M.; Verhagen, R. Advantages of Double Frequency Sweeps in Static, MAS and MQMAS NMR of Spin I=3/2 Nuclei. *Chem. Phys. Lett.* 1999, 300, 435−443.

(72) Comellas, G.; Lopez, J. J.; Nieuwkoop, A. J.; Lemkau, L. R.; Rienstra, C. M. Straightforward, Effective Calibration of SPINAL-64 Decoupling Results in the Enhancement of Sensitivity and Resolution of Biomolecular Solid-State NMR. *J. Magn. Reson.* 2011, 209, 131−135.

(73) Gan, Z.; Hung, I.; Wang, X.; Paulino, J.; Wu, G.; Litvak, I. M.; Gor'kov, P. L.; Brey, W. W.; Lendi, P.; Schiano, J. L.; et al. NMR Spectroscopy up to 35.2 T Using a Series-Connected Hybrid Magnet. *J. Magn. Reson.* 2017, 284, 125−136.

(74) Bielecki, A.; Burum, D. P. Temperature Dependence of ^{207}Pb MAS Spectra of Solid Lead Nitrate. An Accurate, Sensitive Thermometer for Variable-Temperature MAS. *J. Magn. Reson. Ser. A* 1995, 116, 215−220.

(75) Kresse, G.; Furthmüller, J. Efficiency of Ab-Initio Total Energy Calculations for Metals and Semiconductors Using a Plane-Wave Basis Set. *Comput. Mater. Sci.* 1996, 6, 15−50.

(76) Kresse, G.; Hafner, J. Ab Initio Molecular Dynamics for Liquid Metals. *Phys. Rev. B* 1993, 47, 558−561.

(77) Giannozzi, P.; Baroni, S.; Bonini, N.; Calandra, M.; Car, R.; Cavazzoni, C.; Ceresoli, D.; Chiarotti, G. L.; Cococcioni, M.; Dabo, I.; et al. QUANTUM ESPRESSO: A Modular and Open-Source Software Project for Quantum Simulations of Materials. *J. Phys. Condens. Matter.* 2009, 21, No. 395502.

(78) Perdew, J. P.; Burke, K.; Ernzerhof, M. Generalized Gradient Approximation Made Simple. *Phys. Rev. Lett.* 1996, 77, 3865−3868.

(79) Troullier, N.; Martins, J. L. Efficient Pseudopotentials for Plane-Wave Calculations. *Phys. Rev. B* 1991, 43, 1993−2006.

(80) Bylander, D. M.; Kleinman, L. Efficacious Form for Model Pseudopotentials. *Phys. Rev. Lett.* 1982, 48, 1425−1428.

(81) Pickard, C. J.; Mauri, F. All-Electron Magnetic Response with Pseudopotentials: NMR Chemical Shifts. *Phys. Rev. B* 2001, 63, No. 245101.

(82) Kutzelnigg, W.; Fleischer, U.; Schindler, M. The IGLO-Method: Ab-Initio Calculation and Interpretation of NMR Chemical Shifts and Magnetic Susceptibilities. In *Deuterium and Shift Calculation*; Springer, 1990; pp. 165−262.

(83) Pyykkö, P. Year-2017 Nuclear Quadrupole Moments. *Mol. Phys.* 2018, 116, 1328−1338.

(84) Herzfeld, J.; Berger, A. E. Sideband Intensities in NMR Spectra of Samples Spinning at the Magic Angle. *J. Chem. Phys.* 1980, 73, 6021−6030.

(85) Massiot, D.; Fayon, F.; Capron, M.; King, I.; Le Calvé, S.; Alonso, B.; Durand, J.-O.; Bujoli, B.; Gan, Z.; Hoatson, G. Modelling One- and Two-Dimensional Solid-State NMR Spectra. *Magn. Reson. Chem.* 2002, 40, 70−76.

(86) Macho, V.; Brombacher, L.; Spiess, H. W. Applied Magnetic Resonance The NMR-WEBLAB: An Internet Approach to NMR Lineshape Analysis. *Appl. Magn. Reson.* 2001, 20, 405−432.

(87) The Math Works, Inc. *MATLAB*, version 2021b. https://www.mathworks.com/.

(88) Carmona, P. On the Hydrogen Bonding of Whewellite. *Spectrosc. Lett.* 1977, 10, 645−653.

(89) Bowmaker, G. A. Solvent-Assisted Mechanochemistry. *Chem. Commun.* 2013, 49, 334−348.

(90) Mottillo, C.; Friščić, T. Advances in Solid-State Transformations of Coordination Bonds: From the Ball Mill to the Aging Chamber. *Molecules* 2017, 22, 144.

(91) Huskić, I.; Lennox, C. B.; Friščić, T. Accelerated Ageing Reactions: Towards Simpler, Solvent-Free, Low Energy Chemistry. *Green Chem.* 2020, 22, 5881−5901.

(92) Wang, R.; Xu, G.; He, Y. Structure and Properties of Polytetrafluoroethylene (PTFE) Fibers. *e-Polymers* 2017, 17, 215−220.

(93) Werner, R. A.; Brand, W. A. Referencing Strategies and Techniques in Stable Isotope Ratio Analysis. *Rapid Commun. Mass Spectrom.* 2001, 15, 501−519.

(94) Cukierman, S. Et Tu, Grotthuss! And Other Unfinished Stories. *Biochim. Biophys. Acta, Bioenerg.* 2006, 1757, 876−885.

(95) Hung, I.; Wu, G.; Gan, Z. Second-Order Quadrupolar Line Shapes under Molecular Dynamics: An Additional Transition in the Extremely Fast Regime. *Solid State Nucl. Magn. Reson.* 2017, 2017, 14−19.

(96) Ba, Y.; Ripmeester, J. A.; Ratcliffe, C. I. Water Molecular Reorientation in Ice and Tetrahydrofuran Clathrate Hydrate from Lineshape Analysis of ^{17}O Spin-Echo NMR Spectra. *Can. J. Chem.* 2011, 89, 1055−1064.

(97) Chiba, T. Deuteron Magnetic Resonance Study of Some Crystals Containing an O—D⋯O Bond. *J. Chem. Phys.* 1964, 41, 1352−1358.

(98) Chiba, T.; Soda, G. Deuteron Quadrupole Interactions in Two Modifications of Oxalic Acid Dihydrate Crystal. *Bull. Chem. Soc. Jpn.* 1971, 44, 1703−1704.

(99) Pedersen, B.; Håland, K. Isotope Effect in the ^{2}H - NMR-Spectra of Partly Deuterated Hydrates. *Chem. Phys. Lett.* 1968, 2, 61−64.

(100) Mills, S. J.; Christy, A. G. The Great Barrier Reef Expedition 1928−29: The Crystal Structure and Occurrence of Weddellite, Ideally $CaC_2O_4 \cdot 5H_2O$, from the Low Isles, Queensland. *Mineral. Mag.* 2016, 80, 399−406.

(101) Rusakov, A. V.; Frank-Kamenetskaya, O. V.; Gurzhiy, V. V.; Zelenskaya, M. S.; Izatulina, A. R.; Sazanova, K. V. Refinement of the Crystal Structures of Biomimetic Weddellites Produced by Microscopic Fungus Aspergillus Niger. *Crystallogr. Rep.* 2014, 59, 362−368.

(102) Izatulina, A.; Gurzhiy, V.; Frank-Kamenetskaya, O. Weddellite from Renal Stones: Structure Refinement and Dependence of Crystal Chemical Features on H_2O Content. *Am. Mineral.* 2014, 99, 2−7.